SCAR-6 elncRNA locus epigenetically regulates *PROZ* and modulates coagulation and vascular function

Gyan Ranjan[1,2], Paras Sehgal[1,2], Vinod Scaria[1,2,*] Sridhar Sivasubbu [1,2,*]

1. CSIR Institute of Genomics and Integrative Biology, Mathura Road, Delhi 110024, India
2. Academy of Scientific and Innovative Research (AcSIR), Ghaziabad- 201002, India

*Corresponding author:-

Dr. Sridhar Sivasubbu

Chief Scientist,

CSIR Institute of Genomics and Integrative Biology (CSIR-IGIB),

South Campus, Mathura Road, New Delhi 110 025. India

Email:- sridhar@igib.in, sridhar.sivasubbu@gmail.com

Dr. Vinod Scaria

Senior Principal Scientist,

CSIR Institute of Genomics and Integrative Biology (CSIR-IGIB),

South Campus, Mathura Road, New Delhi 110 025. India

Email:- vinod.s@igib.in, drvinod@gmail.com

Abstract

Syntenic conservation is an effective strategy to identify evolutionarily conserved lncRNA orthologs. In this study, we identified a novel uncharacterized conserved lncRNA known as *Syntenic Cardiovascular Conserved Region-Associated lncRNA-6 (scar-6)* and functionally validated its role in coagulation and cardiovascular function. Precise editing of the *scar-6* lncRNA locus in zebrafish (*scar-6*$^{gib007\Delta12/\Delta12}$) resulted in cranial hemorrhage and permeability defects. Further analysis, including overexpression, locus editing, and rescue experiments, provided compelling evidence for the critical role of the *scar-6* transcript in the coagulation process of zebrafish. Notably, rescue attempts were unsuccessful in mitigating cranial hemorrhage. Molecular investigation revealed that the *scar-6* RNA acts as an enhancer lncRNA (elncRNA), and controls the expression of *prozb*, an inhibitor of *factor Xa*, through the enhancer element on its locus. The *scar-6* locus actively suppresses the loop formation between *prozb* and *scar-6* sequences, facilitated by methylation of CpG island via the *prdm14-PRC2* complex, which is stabilized by the *scar-6* elncRNA transcript. Disruption of this mechanism in *scar-6*$^{gib007\Delta12/\Delta12}$ zebrafish led to impaired vascular function and subsequent hemorrhage. This was triggered by the activation of the *PAR2* receptor mediated by upregulation of *prozb*, which in turn caused *NF-κB*-mediated endothelial cell activation. This study presents novel evidence for the multifaceted function of the *scar-6* locus, highlighting its crucial role in regulating the coagulation cascade gene *prozb* and maintaining homeostasis and vascular function.

Keywords

zebrafish, epigenetic, endothelial cell, cardiovascular, hemorrhage, synteny lncRNA, conservation, coagulation

Synopsis

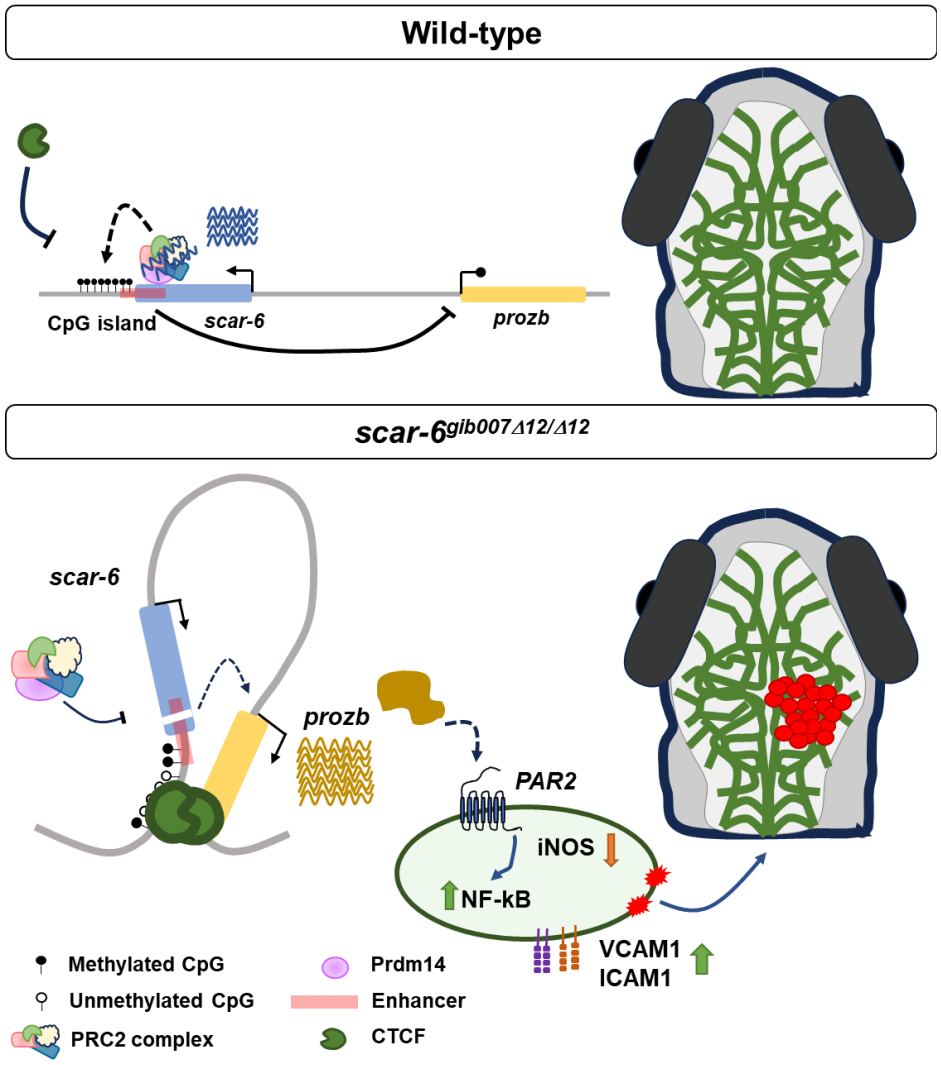

ProZ-PZI is a natural inhibitor of activated *coagulation factor X (F10)* and plays a major role in maintaining hemostasis in-vivo. Here, the novel evolutionary syntenic conserved *scar-6* elncRNA locus is shown to regulate *prozb* expression and control coagulation and vascular integrity in zebrafish.

- The *scar-6* acts as an enhancer lncRNA (elncRNA). It controls *prozb* expression and modulates coagulation and vascular function in zebrafish.
- The *scar-6* elncRNA stabilizes the *Prdm14-PRC2* complex binding to *scar-6* locus. This inhibits *prozb/scar-6* looping via methylating the CpG island under wildtype conditions.
- Overexpressed *prozb* in *scar-6* edited animals activates *PAR2* receptor, causing endothelial cell activation and vascular dysfunction.

Introduction

Long non-coding RNAs (lncRNAs) have been investigated for their functions and have been found to regulate protein-coding genes in *cis* or *trans* in various biological conditions (Kopp & Mendell, 2018; Gil & Ulitsky, 2020). To date, only a handful of lncRNA genes have been functionally characterized using model organisms, such as mice or zebrafish, to understand complex regulatory networks in disease and development (Ranjan *et al*, 2021; Sauvageau *et al*, 2013; Han *et al*, 2018; Sehgal *et al*, 2021; Kurian *et al*, 2016; Hosono *et al*, 2017). Numerous lncRNAs, including *MALAT1, Caren, MANTIS, Mhrt, Tug1,* and *Pnky*, have been shown to be physiologically crucial for organ development, maturation, and function(Cremer *et al*, 2019; Sato *et al*, 2021; Leisegang *et al*, 2017; Lewandowski *et al*, 2020; Ramos *et al*, 2015). These lncRNAs provide compelling evidence of their significant roles in regulating key biological processes, underscoring their importance in maintaining proper organ physiology (Oo *et al*, 2022). However, genomic comparisons of lncRNAs based on nucleotide sequences across vertebrates have shown low or no sequence conservation, posing a significant challenge in identifying orthologs (Hezroni *et al*, 2015). Multiple studies have shown that lncRNAs exhibit alternative conservation modes independent of their sequence (Diederichs, 2014; Ranjan *et al*, 2021). lncRNAs arising from conserved syntenic loci and thus exhibiting functional conservation is one such mode that is frequently used to study lncRNA orthologs. Syntenic loci are evolutionarily conserved regions on a chromosome that exhibit a similar order of homologous genes across different species, primarily defined around protein-coding genes. Several lncRNA orthologs proximal to homologous protein-coding genes have been identified using the conserved synteny approach in different model organisms (Ranjan *et al*, 2021). The availability of large catalog datasets of lncRNAs from zebrafish has recently opened avenues for

understanding the lncRNA-mediated regulatory aspects of conserved developmental and morphological pathways across vertebrates (Hu *et al*, 2018). Multiple investigations have previously identified many syntenically conserved lncRNAs in zebrafish that have shown functional importance. *Tie1-AS, PUNISHER, ALIEN, MALAT1, TERMINATOR, Durga,* and *PU.1 AS* are some lncRNAs arising from syntenic conserved loci that show the presence of functional orthologs between humans and zebrafish (Ranjan *et al*, 2021; Kurian *et al*, 2016; Sarangdhar *et al*, 2017; Li *et al*, 2010; Wei *et al*, 2014; Wu *et al*, 2019; Ulitsky *et al*, 2011).

Additionally, uncovering the functional modalities of these lncRNA locus has been a central focus of the field.

LncRNA loci are categorized based on their mechanisms of action. Some function through their mature RNA molecules, interacting with proteins, RNA, or DNA to regulate cellular processes (e.g., *VEAL2, GATA6-AS, Tie1-AS, lncREST*) (Sehgal *et al*, 2021; Neumann *et al*, 2018; Li *et al*, 2010; Statello *et al*, 2024). Others act through the transcription process, serving as bidirectional promoters or transcription and splicing regulators (e.g., *ARIN, Handsdown*) *(Santoro et al, 2013; Ritter et al, 2019)*. Additionally, some loci operate exclusively through their DNA elements, functioning as chromatin, enhancer, or transcription factor binding regions (e.g., *PVT1, linc-p21, Lockd, Meteor*)(Cho *et al*, 2018; Groff *et al*, 2016; Rom *et al*, 2019; Gil *et al*, 2023). The RNAs produced from these loci are often termed as enhancer RNAs (eRNAs) or enhancer-associated lncRNAs (elncRNAs). They play significant roles in biological processes like vascular function and development. eRNAs are classified into two categories based on their features and polyadenylation (poly-A)(Lam *et al*, 2014; Natoli & Andrau, 2012; St Laurent *et al*, 2015; Li *et al*, 2016). The first class consists of eRNAs that are bidirectional, single-exonic, non-polyadenylated, and short in size. These RNAs are produced from enhancers

and are often considered transcriptional noise or features of enhancers. The second class includes eRNAs or elncRNAs that exhibit characteristics similar to lncRNAs, such as unidirectional transcription, multi-exonic structure, length greater than 500 bp and polyadenylation (Koch *et al*, 2011; Lam *et al*, 2014; Hou *et al*, 2019). These elncRNA exhibits higher enhancer activity due to post-transcriptional processing of these RNAs (Ørom *et al*, 2010; Gil & Ulitsky, 2018; Arner *et al*, 2015; Tan & Marques, 2022). elncRNAs produced from these loci are known to interact with transcription factors (TFs) and stabilize their binding at the locus, thereby mediating transcription. Additionally, eRNAs are involved in phase condensation and methylation via m6A modification, which are critical for active enhancer functions(Mattick *et al*, 2023; Lee *et al*, 2021). The involvement of eRNAs in phase condensates has been reported, underscoring their importance in cellular processes. Moreover, multiple studies have indicated that targeting these elncRNAs can have therapeutic potential, highlighting their relevance in disease contexts(Zhang *et al*, 2019; Allou *et al*, 2021; Cajigas *et al*, 2018; Katsushima *et al*, 2024; Fatima *et al*, 2019; Sun *et al*, 2014).

The cardiovascular system comprises a complex network of tissues that orchestrates blood circulation and other essential components throughout the body. Recent advancements have identified numerous proteins crucial for the maintenance and functionality of vascular and cardiac tissues (Srivastava & Olson, 2000; Trimm & Red-Horse, 2022). Transcriptional regulation within these tissues is pivotal for maintaining systemic homeostasis, and disruptions in these regulatory networks can lead to pathological conditions such as coronary artery disease (CAD), stroke, and heart failure (Spielmann *et al*, 2022; Marsman *et al*, 2013; Anene-Nzelu *et al*, 2021; Mathew & Sivasubbu, 2022; Park *et al*, 2013). Additionally, recent studies have underscored the significance of various coagulation factor proteins in cardiovascular function

(Zhao & Schooling, 2018; Loeffen *et al*, 2012). These enzymes, which contain the serine protease domain, are integral not only to coagulation but also to mediating pro-inflammatory signaling via the activation of protease-activated receptors (PAR1, 2, 3, and 4) (Posma et al., 2019; Heuberger & Schuepbach, 2019). Activating these receptors by clotting factors such as thrombin and FXa can induce endothelial cell activation, leading to vascular dysfunction(Rabiet *et al*, 1996; Bono *et al*, 2000). However, the transcriptional regulation of these proteins remains poorly understood, partly due to the lethality of knockout models for these factors. Zebrafish have recently emerged as a valuable model system for studying coagulation and cardiovascular genetics due to their conserved coagulation cascade and cardiovascular gene networks (Liu et al., 2014; Hu et al., 2017; Weyand et al., 2019). Unlike mouse models, zebrafish can tolerate severe defects during early development, facilitating research on these pathways (Dewerchin et al., 2000; Liu et al., 2014; Cui et al., 1996; Hu et al., 2017; Jalbert et al., 1998). Furthermore, emerging evidence suggests that elncRNAs regulate enhancers or promoters of neighboring protein-coding genes involved in cardiovascular function. Examples of such elncRNAs include *AIRN, Chaserr, Handsdown, Pcdhα-as, Upperhand, GAL10-ncRNA, Haunt, PVT1, and Fxt.* These elncRNAs play crucial roles in modulating gene expression and maintaining cardiovascular homeostasis (Ali & Grote, 2020; Yin et al., 2015; Ritter et al., 2019; Rom et al., 2019; Canzio et al., 2019; Latos et al., 2012; Han et al., 2019; Furlan et al., 2018; Cho et al., 2018; Hosen et al., 2018).

In this study, we genetically probed the role of previously uncharacterized syntenic conserved lncRNA locus *scar-6* in zebrafish and for the first time, provided provided evidence that the *scar-6* lncRNA locus functions as an enhancer, producing an elncRNA transcript that collaboratively regulates the *prozb* gene. It also controls coagulation and vascular function

in-vivo. The *scar-6* locus consists of an enhancer that modulates *prozb* expression via binding of the *prdm14-PRC2* complex at the locus which is stabalized by the *scar-6* elncRNA. The *prdm14-PRC2* complex modulates the methylation of nearby CpG island, affecting the CTCF binding and enhancer (*scar-6*)-promoter (*prozb*) looping. Moreover, the upregulation of *prozb* in the mutant *scar-6* zebrafish resulted in the activation of the *PAR-2* receptor, causing upregulation of *ICAM1* and *VCAM1* expression, leading to vascular dysfunction. This study puts forward the role of *scar-6* elncRNA locus in modulating coagulation and vascular function via controlling the expression of the *prozb* gene.

Results

Identification of syntenic lncRNA genes associated with the cardiovascular system

We used a systematic approach to identify syntenic conserved lncRNA genes in the cardiovascular system. Using the genome map in the ZFLNC database (Hu *et al*, 2018), we listed out 5 neighboring protein-coding genes of all syntenic lncRNA genes in zebrafish (337 lncRNA genes) and obtained a total of 571 neighboring protein-coding genes. We compiled a comprehensive list of cardiovascular system-associated genes by querying the Zfin database with keywords such as "heart" (2531 genes), "blood vessels" (1122 genes), and "endothelium" (287 genes) (Bradford *et al*, 2022). This process resulted in a consolidated list comprising 2854 protein-coding genes. We then overlapped the 571 protein-coding genes proximal to syntenic lncRNAs with the cardiovascular-associated gene lists (2854 genes). We found 291 overlapping protein-coding genes in proximity to 98 syntenic lncRNA genes. To enhance the likelihood of identifying syntenic lncRNA genes involved in the cardiovascular system, we excluded those with only one adjacent protein-coding gene. We focused on retaining syntenic lncRNA genes that had multiple neighboring protein-coding genes associated with cardiovascular functions. We

also excluded lncRNAs that were single exonic transcripts and retained multiexonic lncRNAs (58 lncRNA gene) (Andersson *et al*, 2014). Additionally, we selected lncRNAs that had single predicted human ortholog transcripts to avoid any potential confusion (36 lncRNA gene) and further refine our selection process by prioritizing candidate lncRNAs based on the Mendelian disease associations of their neighboring genes and got 10 potential syntenic conserved lncRNAs with possible involvement in the cardiovascular system. (Supp table S2). We named the selected lncRNA genes as *Syntenic Cardiovascular Conserved Region-Associated lncRNA (scar)* (Fig 1A) (Supp Fig 1A)**.**

scar-6 is a novel uncharacterized conserved lncRNA gene

We selected *scar-6* lncRNA gene as a candidate for functional validation as it belongs to a highly conserved syntenic block comprising the genes involved in the coagulation cascade, and no lncRNA has been previously characterized for its functional association with coagulation and the cardiovascular system, making it a novel target for our investigation. The *scar-6* lncRNA locus produces a bi-exonic polyadenylated lncRNA (Fig EV1A). It has a transcript length of 632 bp observed in a synteny block on chromosome 1 of zebrafish and arises antisense to 3'UTR of the *coagulation factor X* (*f10)* gene and upstream to *protein zb* (*prozb)* gene (Fig 1B). Strand-specific PCR and 3'- rapid amplification of cDNA ends (RACE), and strand specific amplification conform *scar-6* to be an independent antisense transcript to the *f10* gene (Fig 1B) (Supp Fig 2). The *scar-6* lncRNA locus has a putative syntenic conserved locus in humans which also produces bi-exonic novel transcript, antisense to *F10* (ENSG00000283828) (previously named *AL137002.2* or *LOC102724474*) (hereafter mentioned as *SCAR-6).* It is present in the human conserved syntenic block on chromosome 13 with length of 2238 bp and antisense to the

F10 gene, overlapping with its 3'UTR and upstream to *PROZ* gene (Fig 1C). It shows no sequence conservation with its putative zebrafish orthologue (Supp Fig 3-4). We also computed the non-coding potential of the lncRNAs using bioinformatic algorithms such as the Coding Potential Assessment Tool (CPAT2) (coding probability - 0.0003) (Wang *et al*, 2013) or Coding Potential Calculator (CPC2) (coding probability - 0.0192227) (Kang *et al*, 2017), and found *scar-6* lncRNA to exhibit no coding potential (Fig EV1B). Additionally, sub-cellular investigation for *scar-6* lncRNA and its neighboring genes in zebrafish showed enrichment of *scar-6* and *prozb* expression in the nuclear compartment. In contrast, *f10* showed expression in both the cytoplasmic and nuclear compartments (Fig EV1C-D). Subsequently, we conducted expression analysis of *scar-6* and adjacent genes by re-analyzing RNA-seq datasets from developmental stages and adult tissues, which are publicly accessible (Pauli *et al*, 2012; Yang *et al*, 2020; Sehgal *et al*, 2021). We observed *scar-6* to be expressed from the bud stage to 5dpf. It showed a similar expression pattern to *f10* after 28hpf and no primary pattern was observed for *prozb* throughout the developmental stages (Fig 1D). We observed *scar-6* to be ubiquitously expressed in 11 of the tested 12 zebrafish adult tissues and show higher expression in the liver. The expression of neighboring genes *f10* and *prozb* showed relatively very low expression in selected tissues (Fig 1E). As both *f10* and *prozb* are expressed and secreted out from the liver (Heinz & Braspenning, 2015; Kemkes-Matthes & Matthes, 1995), we also observed similar expression of *scar-6* lncRNA and its neighboring protein-coding genes in our expression analysis. *In situ hybridization* at 3dpf and 5dpf of zebrafish showed a concordant expression pattern of *scar-6* lncRNA in zebrafish (Fig 1F)(supp Fig 5). Similar tissue expression patterns were also observed in human tissues in the GTEx v8 database for the *SCAR-6* lncRNA gene (Ferraro *et al*, 2020) (Fig EV1E)**.** This data indicates that the *scar-6* locus produces an RNA

transcript exhibiting typical characteristics of lncRNAs, including non-coding nature, biexonic structure with a poly-A tail, and a length greater than 500 bp.

The *scar-6* locus modulates vascular and hemostasis function.

To understand the function of *scar-6* locus in the coagulation cascade and cardiovascular system, we generated a stable mutant line using the CRISPR-Cas9 system. We designed sgRNAs targeting the 1st and 2nd exon of *scar-6* lncRNA gene in a double transgenic zebrafish *gib004Tg*(*fli1: EGFP; gata1a:dsRed*) background (Lalwani *et al*, 2012; Lawson & Weinstein, 2002; Traver *et al*, 2003). In our initial F_0 screening, we observed no phenotype in the cardiovascular system of zebrafish crispants targeted for exon 1. However, we noted cranial hemorrhage in approximately 30% of crispants with the sgRNA targeting the 2nd exon (3' region) of the *scar-6* gene. Therefore, we selected these mutants for further study. (supp Fig 6). We used a systematic approach to generate a stable F_2 mutant animal line with a 12-bp deletion in exon 2 at position 594-606 bases of *scar-6* transcript and named it *scar-6*$^{gib007\Delta12}$ (detailed in supplementary data section) (Fig 2A-B) (Fig EV2A) (Supp Fig 7). The *scar-6*$^{gib007\Delta12/+}$ animals were checked for morphological or patterning defects in the cardiovascular system till 5dpf in double transgenic background zebrafish (*gib004Tg*(*fli1: EGFP; gata1a:dsRed*)) under a fluorescent microscope. We observed no significant defects in patterning and formation of blood vessels. We next in-crossed two *scar-6*$^{gib007\Delta12/+}$ animals and observed the progeny displaying genotype in the mendelian ratio (Fig 2C,D). Upon further investigation, we observed that 22.7% (P-value=0.0023, unpaired two-tail t-test) of the offspring exhibited cranial hemorrhage phenotype starting from 60 hpf and prominent at 72 hpf (3dpf) (Fig 2C,E). Subsequently, upon genotyping these hemorrhage animals from three independent in-crosses of *scar-6*$^{gib007\Delta12/+}$ animals demonstrated that 96% (86/90) of the animals carried the homozygous mutation (Fig

2G). This suggests that homozygous mutant animals of *scar-6*$^{gib007\Delta12/\Delta12}$ exhibit cranial hemorrhage phenotype (Fig 2F). We also observed the embryos under a confocal microscope and fluorescent microscope to understand the cause of hemorrhage, but we did not find any visible vascular malformations or patterning defects in the mutant zebrafish (Fig EV2B). To further characterize, we checked for any permeability defect in our mutant by injecting Evans blue dye into the zebrafish's common cardinal vein (CCV). Notably, *scar-6*$^{gib007\Delta12/\Delta12}$ animals exhibited permeability defects, evidenced by dye leakage between the intersegmental vessels (ISV). This observation strongly indicates that the permeability defect in *scar-6*$^{gib007\Delta12/\Delta12}$ animals led to hemorrhage (Fig 2 H-I).

Next, we examined the molecular alterations in the zebrafish mutant of the *scar-6* lncRNA. We observed that there was an 8-fold increase in the expression of the upstream neighboring gene *prozb* in the *scar-6*$^{gib007\Delta12/\Delta12}$ animals when compared to the wild-type counterparts (p-value $\leq$ 0.001, unpaired two-tailed t-test). However, we did not find any significant changes in the expression levels *f10 and scar-6* when comparing the *scar-6*$^{gib007\Delta12/\Delta12}$ animals to the wild-type counterparts. (Fig 2J). This implies that the *scar-6* locus functions in a *cis*-regulatory manner, specifically influencing *prozb* expression. The unchanged levels of *scar-6* lncRNA suggest that the 12-bp deletion may not affect its degradation but could potentially alter its secondary structure, thereby disrupting its functional role. Therefore, we examined the secondary structure of the lncRNA with and without the 12-bp deletion using RNAfold web server (Lorenz *et al*, 2011). We observed a significant alteration in the secondary structure of the lncRNA following the deletion of 12 bp (Fig EV2C). The observed changes, particularly in the hairpin loop structure, could profoundly impact the *scar-6* lncRNA's function. This structural alteration might affect its ability to interact with target molecules, regulate gene expression, and

stabilize transcription factor binding at the regulatory site. These disruptions could render the *scar-6* lncRNA nonfunctional, explaining the observed changes in *prozb* expression.

We further evaluated the hemostasis ability of *scar-6* in the zebrafish. We in-crossed the *scar-6*$^{gib007\Delta12/+}$ animals and the embryos were further subjected to a mechanical vascular injury at the cardinal vein (CV) of 3dpf animals. The occlusion time was recorded blindly, and subsequent genotyping was performed (Clay & Coughlin, 2015). We observed a significant loss of hemostasis ability in both heterozygous (*scar-6*$^{gib007\Delta12/+}$) and homozygous (*scar-6*$^{gib007\Delta12/\Delta12}$) mutants of *scar-6* animals. The mean occlusion time was 40.5 seconds for heterozygous mutants and 120 seconds for homozygous mutants, compared to only 24.5 seconds for the control group. (p-value < 0.0001, Mann Whitney *U* test) (Fig 3A). We also analyzed the hemostasis ability upon overexpression of the wild-type *scar-6* lncRNA in zebrafish and recorded the occlusion time blindly upon mechanical vascular injury at the CV. We injected 3 different concentrations (100 ng/uL, 200 ng/uL, and 500 ng/uL) of the *scar-6 in-vitro* transcribed (IVT) RNA into the single-cell wild-type zebrafish (Supp Fig 9). We observed a significant enhancement of hemostasis in a dose-dependent manner when *scar-6* lncRNA was overexpressed, suggesting its probable role in hemostasis (p-value < 0.0001, Mann-Whitney *U* test)(Fig 3B).

Knockout models of coagulation cascade genes in mice have been characterized as embryonic lethal (Dewerchin *et al*, 2000; Cui *et al*, 1996; Denis *et al*, 1998). Also, recent studies in zebrafish suggest that knockouts of coagulation cascade genes are embryonic viable but exhibit adult lethality (Liu *et al*, 2014; Hu *et al*, 2017; Weyand *et al*, 2019). Therefore, we investigated the survival rate of *scar-6*$^{gib007\Delta12/\Delta12}$ zebrafish embryos for 6 months. We observed that the wild-type animals exhibit a normal survival rate of 80%. In contrast, the *scar-6*$^{gib007\Delta12/\Delta12}$ animals displayed a significant reduction in survival rate, with only 20% of them surviving

(p-value <0.0001, log-rank test)(Fig 3C). We conducted a morphological assessment of the animals during the survival analysis at 30 days post-fertilization (dpf). Notably, we observed that the homozygous mutants exhibited carinal hemorrhage defects of varying severity, mainly categorized as severe, moderate, and minimal (Fig 3D, E)(Supp Fig 8).

To exclude the possibility that *f10* disruption contributes to the observed phenotype, we evaluated both mRNA and protein levels of *f10* and found no significant alterations. (Fig 2J, Supp Fig 9A). Additionally, a rescue experiment by overexpressing *f10* mRNA IVT (100 ng/µL) in both wild-type and *scar-6*$^{gib007\Delta12/\Delta12}$ animals showed no rescue of the phenotype suggesting no involvement of *f10* in the observed phenotype of *scar-6* mutant. (Supp Fig 9B, C).

Scar-6 acts as enhancer lnRNA and exhibits _cis_-regulatory function.

We next evaluate the functional modality of the *scar-6* locus. We attempted to rescue the phenotype of *scar-6*$^{gib007\Delta12/\Delta12}$ animals by injecting wild-type *scar-6* IVT RNA (100 ng/µL) into the progeny of in-crossed *scar-6*$^{gib007\Delta12/+}$ animals. We assessed the hemostatic ability of the mutants after rescue with either the wild-type or 12 bp deleted *scar-6* lncRNA IVT RNA. Our results showed that the in-crossed *scar-6*$^{gib007\Delta12/+}$ animals could restore hemostatic function with the wild-type copy of *scar-6*, but not with the 12 bp deleted copy (Fig 3F). Additionally, there was no change in the percentage of animals with the hemorrhage phenotype (Fig 3G, H) and no molecular change in the expression of *prozb* (Fig 3I).

To further investigate the role of the *scar-6* lncRNA, we conducted a transient knockdown using an anti-sense splice-blocking morpholino (Supp Table S3). We observed no prominent cardiovascular phenotype until 5 dpf upon knockdown (Fig EV3A, B, C). Although a cranial hemorrhage phenotype was observed in a few animals at 3 dpf, the numbers were not significant (Fig EV3C, D). Additionally, there was no change in the expression levels of *f10* and

prozb upon *scar-6* lncRNA knockdown or overexpression (Fig EV3E, Supply Fig 10B). However, a significant change in hemostasis efficiency was noted upon knockdown of the *scar-6* lncRNA (Fig EV3F). These findings indicate that the RNA produced from the *scar-6* locus plays a role in regulating the hemostatic ability of zebrafish.

Taken together these observations suggests the RNA produced from the *scar-6* locus does not appear to impact cranial hemorrhage morphology or significant change in the transcriptional regulation of the *prozb* gene in *scar-6*$^{gib007\Delta12/\Delta12}$ animals. We speculate that the function of the *scar-6* lncRNA may be context-dependent in its role in controlling cranial hemorrhage and *prozb* regulation. Alternatively, other regulatory elements, possibly enhancer, might be involved in regulating *prozb* expression and cranial hemorrhage in the *scar-6* mutants.

Further we evaluate the presence of a DNA regulatory element as the functional modality of the *scar-6* locus. We observed that the *scar-6* lncRNA locus was overlapping with an annotated enhancer region at the 2nd exon of the lncRNA loci, which is active during the prim-5 and log pec stage of zebrafish (Baranasic *et al*, 2022). (Fig 4A) (supply Fig 11). We also observed that in humans, the *SCAR-6* loci exhibited an overlap with distal enhancers (known as CRE) as annotated by ENCODE datasets (ENCODE Project Consortium *et al*, 2020). Moreover, examining chromatin state marks across various human cell lines further confirmed the active regulatory function of the *SCAR-6* locus in a cell line-specific manner (Roadmap Epigenomics Consortium *et al*, 2015) (Fig 4B) Additionally, we investigated the TF binding sites on the *scar-6* locus, considering both human and zebrafish species and found 68 TF which were showing multiple binding sites and enrichment in both human and zebrafish *scar-6* locus (Supp Fig 12). These TF upon gene ontology analyses for biological significance were majorly enriched in embryonic organ morphogenesis, heart looping, cranial development, and other developmental

processes (Supp Fig 12 D). To further validate the locus as an enhancer, we performed an enhancer assay by cloning the zebrafish *scar-6* and human *SCAR-6* locus DNA before a minimal promoter E1b followed by an eGFP reporter and injected it in the single-cell embryo of zebrafish. We observed eGFP signals in the cardiac region of injected animals for both zebrafish *scar-6* and human *SCAR-6* enhancer plasmid. eGFP signal in the trunk region of zebrafish was also observed in animals injected with human *SCAR-6* enhancer plasmid (Fig 4C). Furthermore, we also performed the reporter enhancer assay in human cell culture models using psiCHEK-2 plasmid. We cloned the human *SCAR-6* and zebrafish *scar-6* locus DNA upstream to the SV40 promoter which drives the renilla luciferase (hRluc) and used the firefly luciferase (hluc) driven by HSV-TK promoter to normalize the expression. The plasmids were transfected in HHL-17, HEK297T, HUVEC/tert2, and HepG2 cell lines. We observed that the human *SCAR-6* locus exhibits an enhancer function in HepG2 and HUVEC/hTert2 cells whereas it exhibited a repressor function in the cell lines HHL-17 and HEK297T cell lines after normalization. This was also concordant to the epigenome chromatin marks of HepG2 and HUVEC cells showing enhancer mark and other cell-lines showing quiescent marks (Roadmap Epigenomics Consortium *et al*, 2015) (Fig 4A). Interestingly we did not find any change in the expression with the plasmid containing zebrafish *scar-6* DNA locus in human cell cultures (Fig 4D). The enhancer assay in zebrafish, luciferase assay in cell lines, and associated chromatin marks on the *scar-6* lncRNA gene body in both human and zebrafish collectively suggest that the *scar-6* locus also functions as an enhancer element which regulates *prozb* expression.

The *scar-6* locus regulates *prozb* expression through the *prdm14-PRC2* complex.

Next, we conducted an experiment to assess the functional impact of transcription factors binding at the *scar-6* locus using the CRISPR-dCas9-KRAB complex along with the same

sgRNA targeting the 12 bp mutation region. Notably, we observed a similar hemorrhage phenotype in ~30% of the animals that survived beyond 3 dpf after injection with dCas9-KRAB-sg*scar-6*. In contrast, the control group injected with dCas9-KRAB only showed no such hemorrhage phenotype. These findings support the hypothesis that the observed hemorrhage phenotype is specifically attributed to the precises editing of the enhancer at the *scar-6* locus or locus-specific inhibition of transcription factor binding at the enhancer present on *scar-6* locus. (Fig EV4).

Throughout the development process, it has been observed that distal enhancers play a crucial role in achieving cell type specificity by interacting with promoters through sub-TAD looping. Therefore, we next investigated if the enhancer element in the *scar-6* lncRNA locus and *prozb* gene promoter exhibit any potential looping between them. Using the Hi-C data from human HepG2 cell lines at 10 kb resolution obtained from the ENCODE project (ENCODE Project Consortium *et al*, 2020; Wang *et al*, 2018) and zebrafish brain Hi-C data at 5kb resolution (Yang *et al*, 2020), we observed the presence of sub-TAD looping interactions between the *scar-6* enhancer locus and the *prozb* gene promoter in both human and zebrafish genomes indicating conserved physical interactions between *scar-6/prozb*.(Fig EV 5A)(supp Fig 13-14). To validate the looping, we further performed a chromosome conformation capture (3-C) experiment followed by qPCR specific to the *scar-6* enhancer locus and the *prozb* gene promoter. We observed that the *scar-6*$^{gib007\Delta12/\Delta12}$ animals exhibit an increase in the subTAD-looping when compared to the wild-type animals (Fig 4E). As CTCF-cohesin plays a major role in intra-TAD associations, we also looked into the CTCF binding site at the *scar-6* locus using the publicly available CTCF-ChIP seq data of zebrafish; we observed that at 24 hpf CTCF binding.(Pérez-Rico *et al*, 2020) We observed the presence of CTCF binding at the *scar-6*

and the *prozb* locus (Fig EV5B). We further validated the CTCF occupancy at the *scar-6* locus by performing ChIP-qRT-PCR. Compared to wild-type animals, we observed an enhanced CTCF occupancy at the *scar-6* locus in *scar-6*$^{gib007\Delta12/\Delta12}$ animals (Fig EV5C). This suggests that the upregulation of *prozb* expression in *scar-6*$^{gib007\Delta12/\Delta12}$ animals is due to an increase in CTCF occupancy causing an increase in the looping between the *scar-6* enhancer and *prozb* promoter.

Next, we examined the 68 TF which were showing multiple binding sites at the *scar-6* locus obtained previously and we observed that the 12-bp deletion in *scar-6*$^{gib007\Delta12/\Delta12}$ animals encompassed the *prdm14* binding motif site and could possibly disrupt the binding of it (Fig 5A). We further evaluated the *prdm14* binding at the *scar-6* locus using streptavidin-tagged DNA pulldown assay followed by immunoblotting using a specific *prdm14* antibody. Our experimental results revealed the presence of a distinct band, indicating the direct interaction between *prdm14* and the *scar-6* gene DNA locus. However, this band was notably absent in the *scar-6*$^{gib007\Delta12/\Delta12}$ gene DNA locus, indicating that the 12 bp deletion perturbed the binding of *prdm14* to the *scar-6* locus (Fig EV5D). We also performed ChIP-qPCR to assess the binding of *prdm14* protein at the *scar-6* locus in both wild-type and *scar-6*$^{gib007\Delta12/\Delta12}$ animals. We observed that *prdm14* binding was enriched in the wild-type zebrafish but didn't show any enrichment in the *scar-6*$^{gib007\Delta12/\Delta12}$ zebrafish (Fig 5B). These findings together provide strong evidence that *prdm14* preferentially binds to the *scar-6* locus and is disrupted upon 12-bp deletion. As previous studies have shown that *prdm14* exhibits regulation of the target gene through methylation, we also investigated the methylation pattern of the nearby CpG island using targeted bisulfite sequencing. Our analysis revealed a partial decrease in methylation levels from 100-95% in wild-type animals to 85-78% in *scar-6*$^{gib007\Delta12/\Delta12}$ animals (Fig 5C). Upon further investigation, we observed that the CTCF binding at the *scar-6* locus also overlapped the CpG island. Hence, these data together suggest

that the *scar-6* enhancer region is a sensitive region where the partial decrease in the CpG methylation caused by 12-bp deletion of the *prdm14* motif, leads to an increase in CTCF occupancy.

Previous investigations have demonstrated that elncRNAs originating from the regulatory loci have the ability to recruit or stabilize the binding of transcription factors at their specific loci. (Li *et al*, 2013; Hsieh *et al*, 2014; Pnueli *et al*, 2015; Ivaldi *et al*, 2018; Islam *et al*, 2023; Oksuz *et al*, 2023). Given the previous understanding of *Prdm14* as a repressor that recruits the *PRC2* complex to the target region, we investigated whether the *scar-6* elncRNA transcripts derived from the loci of *scar-6*, have any potential role in the recruitment or interaction with these proteins.(Payer *et al*, 2013; Yamaji *et al*, 2013). To explore this, we performed RNA immunoprecipitation (RIP) followed by qRT-PCR using antibodies against *prdm14* and *Suz12* (protein from *PRC2* complex) in zebrafish. Remarkably, we observed significant enrichment of *scar-6* transcript binding with both *prdm14* and *Suz12* proteins when compared to the IgG control. These findings suggest that *scar-6* elncRNA interacts with the *prdm14-PRC2* complex (Fig 5D). Further to investigate into the role and interaction between *scar-6* lncRNA and *prdm14*, we utilized a morpholino to knockdown the lncRNA and assessed the binding efficiency of prdm14 at the *scar-6* locus. The results revealed a notable ~50% reduction in *prdm14* binding following the lncRNA knockdown (Fig 5E). These findings together suggest *scar-6* elncRNA interacts with the *prdm14-PRC2* complex and may potentially be involved in stabilizing these TF at its locus. (Fig5 F).

PAR2-mediated NF-kβ signaling induces endothelial cell activation and vascular dysfunction.

Coagulation cascade genes such as *FX* and thrombin have a serine protease domain that interacts with protease-activated receptors (PAR) to initiate endothelial cell activation causing an increase in the surface adhesion molecule. This leads to the initiation of atherosclerotic lesions and to vascular dysfunction in the organisms. (Willis Fox & Preston, 2020; Heuberger *et al*, 2019; van den Eshof *et al*, 2017; Alberelli & De Candia, 2014). Structurally, *PROZ* also harbors the serine protease domain which is conserved across species and hypothetically can activate these PAR receptors (Sejima *et al*, 1990). To understand if the *prozb* can also activate endothelial cells and cause hemorrhage, we overexpressed *prozb* in zebrafish. We observed hemorrhage in the cranial region of the zebrafish similar to the *scar-6*$^{gib007\Delta12/\Delta12}$ animals (Fig 6A). We also found a proportion of embryos with trunk development defects (Fig 6B). We next checked if endothelial cells are activated by looking at the levels of different PAR receptors (*PAR1, PAR2a, PAR2b, PAR3*) in our zebrafish mutants. We observed that the levels of *PAR2a* and *PAR2b* were 2-fold upregulated in the *scar-6*$^{gib007\Delta12/\Delta12}$ animals when compared to the wild type (Fig 6C). Next, to check the cleavage of PAR2 *in vivo*, we performed a protease assay. We created a plasmid expressing a protein complex of GFP and Luciferase linked with the PAR2 cleavage domain(Byskov *et al*, 2020). We injected the IVT product of the GFP-PAR2-Luciferase (100ng/ul) into the single-cell embryos of wild-type and incrossed *scar-6*$^{gib007\Delta12/+}$ zebrafish. We observed a increase in the protease activity of the PAR2 domain in the *scar-6*$^{gib007\Delta12/\Delta12}$ animals when compared to the wild-type which was in accordance with the increase in the *PAR2a* and *PAR2b* expression levels in the *scar-6*$^{gib007\Delta12/\Delta12}$ animals (Fig 6D). This implies that upregulated levels of *prozb* in *scar-6*$^{gib007\Delta12/\Delta12}$ zebrafish activates the *PAR2* receptor. Next, we looked into the

downstream pathway by which the activation of the *PAR2* receptor leads to vascular dysfunction. We looked into the levels of one of the downstream proteins NF-kβ, which has been previously reported to be upregulated upon *PAR2* activation (Heuberger *et al*, 2019; Sriwai *et al*, 2013; Minami *et al*, 2003, 2004). We observed that in our *scar-6*$^{gib007\Delta12/\Delta12}$ animals, the protein level of NF-kβ were upregulated compared to the wild type (Fig 6E). Next, we looked into the expression levels of downstream target genes which are activated by NF-kβ and also associated with vascular functioning. We found the expression levels of *vcam2b* and *icam1* to be upregulated whereas the levels of iNO2a were downregulated in our *scar-6*$^{gib007\Delta12/\Delta12}$ animals(Fig 6F). However, we did not observe any significant changes in other downstream target genes of NF-kβ associated with vascular functioning(Supp Fig 15). These findings are consistent with previous reports indicating that activation of the *PAR2* receptor can lead to the activation of NF-kβ, resulting in the upregulation of adhesion molecules such as *VCAM1* and *ICAM1(Byskov et al, 2020; Sun et al, 2021; Minami et al, 2004; Bae & Rezaie, 2009; Buddenkotte et al, 2005)*. We hypothesise that the upregulated expression of these adhesion molecules may contribute to endothelial activation, leading to increased platelet adhesion to the endothelial cell surface(Bombeli *et al*, 1998). This pro-atherogenic effect could potentially explain the observed hemorrhage phenotype in *scar-6*$^{gib007\Delta12/\Delta12}$ animals (Fig 6G) (Nakashima *et al*, 1998; Walpola *et al*, 1995; Heuberger & Schuepbach, 2019).

Discussion

Poor sequence conservation in long noncoding RNA (lncRNA) necessitates exploring alternative modes of evolutionary conservation. In this study, we investigated the functional role of a novel uncharacterized lncRNA locus called *scar-6* identified through a systematic approach in finding an lncRNA locus associated with cardiovascular function. Here, we report for the first

time a lncRNA locus that functionally modulates coagulation and vascular function *in-vivo*. Interestingly, we observed that the RNA produced from the *scar-6* locus exhibits no sequence conservation with its putative human ortholog, although the locus itself is syntenic and functionally conserved. Dissecting the functional modality of the *scar-6* locus - whether as an RNA molecule, the act of transcription, or a DNA regulatory element - is intricate, as many lncRNA loci have demonstrated complex functions, exhibiting single or multiple functional modalities(Gil *et al*, 2023; Lewandowski *et al*, 2020; Andergassen *et al*, 2019; Santoro *et al*, 2013; Yin *et al*, 2015; Sehgal *et al*, 2021; Ritter *et al*, 2019; Wang *et al*, 2011). Functional assays, including knockdown, overexpression, locus editing, and complementation with the wild-type *scar-6* RNA copy in *scar-6*$^{gib007\Delta12/\Delta12}$ animals, have elucidated that the *scar-6* locus encompasses a cell-type-specific distal enhancer, and also produces an RNA transcript that functions as an enhancer lncRNA. This elncRNA stabilizes the binding of transcription factors at the enhancer site on the *scar-6* locus. Although the *scar-6* RNA is involved in modulating in vivo hemostatic function, it did not show any independent impact on cranial hemorrhage. These findings underscore that the *scar-6* locus's function is mediated by both its DNA elements and the elncRNA it produces.

Moreover, the *scar-6* enhancer exhibits a regulatory effect on the *cis* protein-coding gene *prozb*. Bioinformatic analysis also suggests enrichment of DNA elements on the locus of syntenic conserved *scar-6* elncRNA locus between humans and zebrafish with sequence divergence (Ranjan *et al*, 2024). Previous functional studies have indicated that enhancer-associated syntenic conserved lncRNAs exhibit low sequence conservation, implying limited evolutionary constraints on these noncoding regions (Hezroni *et al*, 2015; Gil *et al*, 2023; Paralkar *et al*, 2016; Rom *et al*, 2019). Furthermore, our detailed examination revealed that the

scar-6 gene locus partially overlaps with a conserved CpG island, with no sequence similarity. This CpG island in zebrafish is enriched with *prdm14* binding motifs, while in humans, it is enriched with *PRDM9* binding motifs that overlap with a tandem GC repeat region (supp Fig 16). This raises a possibility that transposable elements-mediated rearrangements of the *scar-6* locus during evolution could have led to the gain or replacement of functional elements to adapt to the complex functioning of larger mammals (Modzelewski *et al*, 2022; Shapiro, 2014; Ciliberti *et al*, 2007; Ranjan *et al*, 2024). It might also provide a potential explanation for the enhancer signal observed in other regions of zebrafish injected with the plasmid containing the enhancer of the human *SCAR-6* locus. This type of vertebrate genome innovation has been previously reported between zebrafish and humans describing diversity in the function of noncoding regulatory regions. (Bedell *et al*, 2012; Lowe *et al*, 2011; Douglas & Hill, 2014; McEwen *et al*, 2009)

Multiple studies have demonstrated that RNA produced from the enhancer or promoter locus are called enhancer RNA(eRNA) or enhancer lncRNA based on the transcript characteristics and features. Briefly eRNA are transcript with single exon and bidirectional transcription and no poly A making it short lived. The other class of eRNA can be associated with the recruitment or stabilizing the binding of TF at the locus (Sigova *et al*, 2015; Andersson *et al*, 2014). Hence, based on RIP-qPCR data, the *scar-6* RNA could possibly recruit or stabilize the transcription factor *prdm14* and *PRC2* complex (*Suz12*) at the *scar-6* enhancer locus. Interestingly recent studies have highlighted that an organism exhibits certain regions in the genome that are sensitive to gene transcription regulation and are generally modulated by the recruitment of a specific class of transcription factors called co-repressors at the enhancer locus to control the gene expression (Jacobs *et al*, 2023; Schertzer *et al*, 2019). Additionally, the

correlation between lncRNA potency, abundance, and PRC2 recruitment to CpG islands within lncRNA-targeted domains suggests a potential model. In this model, CpG islands autonomously attract PRC2 and interact with lncRNAs and their associated proteins in three-dimensional space, initiating the spread of PRC2 within these domains via lncRNA-independent mechanisms (Jacobs *et al*, 2023; Schertzer *et al*, 2019). In our study, we also observed a similar pattern whereupon disruption of the binding site of *prdm14-PCR2* complex (co-repressor) resulted in upregulation of the target gene *prozb,* leading to hemorrhage in the animals. This was in accordance with previous studies where the *prdm14-PCR2* complex has been associated with a repressor function where they modulate the expression of their target genes by methylating the CpG island nearby potentially involving Dnmt1 (Viré *et al*, 2006; Li *et al*, 2015). With these, we hypothesize that the *scar-6* locus is a sensitive region in the genome that modulates the expression of *prozb* gene by recruitment of the *prdm14-PRC2* complex as a co-repressor at its locus. The *prdm14-PRC2* complex represses the expression of *prozb* by methylating the nearby CpG island inhibiting the binding of CTCF to the locus and hampering the *scar-6* enhancer /*prozb* promoter looping (Fig 7).

While only a few lncRNA locus have been associated with disease progression, a significant proportion of disease-related noncoding locus remain uncharacterized due to their complex manifestations, requiring the use of model organisms to decipher their functions (Feyder & Goff, 2016; Allou *et al*, 2021; Ishii *et al*, 2006; Vollmers *et al*, 2021; Sato *et al*, 2021). Interestingly, there have been no previous reports linking elncRNA locus to coagulation-related diseases, and investigations of coagulation-associated genes in mouse models have proven to be lethal. (Jalbert *et al*, 1998; Ishiguro *et al*, 2000; Cui *et al*, 1996; Dewerchin *et al*, 2000; Weyand *et al*, 2019; Hu *et al*, 2017; Liu *et al*, 2014) However, zebrafish models have exhibited a certain

degree of tolerance to knockout of coagulation genes, making them suitable for studying such genes (Liu *et al*, 2014; Hu *et al*, 2017; Weyand *et al*, 2019). In this study, we identified and characterized a novel elncRNA locus associated with hemostasis regulation. Precious editing of the elncRNA *scar-6* locus result in a hemorrhagic phenotype during early development, similar to the characteristic phenotype observed in coagulation-associated protein-coding genes (Hu *et al*, 2017; Weyand *et al*, 2019; Liu *et al*, 2014).

In the *scar-6* mutant, we did not observe any change in the expression of *f10* gene but found the *prozb* gene to be 8-fold upregulated. Prior research has emphasized the significant role of the *PROZ-ZPI* complex in regulating the activated *F10* proteins, which is a crucial gene in the pathway(Han *et al*, 2000, 1998; Sofi *et al*, 2004). Coagulation protein levels must be tightly controlled in a stoichiometric ratio in normal physiological conditions. The *scar-6* lncRNA emerges as a critical and sensitive regulator of *prozb*, the primary inhibitor of *f10* protein. This highlights the crucial role of *scar-6* lncRNA in the coagulation pathway. Notably, we observed that the hemorrhage occurs early in *scar-6* locus mutants, This observation was similar to the late manifestation of hemorrhage in zebrafish knockouts for protein-coding coagulation genes such as *factor 10*, *factor V,* or *antithrombin III*, which typically occur during the juvenile or adult stages. Interestingly, we did not observe widespread hemorrhage similar to $f10^{-/-}$ mutants in $scar\text{-}6^{gib007\Delta12/\Delta12}$ animals (Hu *et al*, 2017), and the expression level of *f10* remained unchanged. This suggests that the function of *f10* in the mutant was not altered. The molecular investigation provided insight that upregulation of *prozb* leads to activation of the *PAR2* receptor pathway causing vascular dysfunction and stroke-like phenotype. This finding aligns with previous reports in humans that have indicated altered levels of *Proz* in similar stroke-like phenotypes. (Zhang *et al*, 2017; Staton *et al*, 2005) Although the exact mechanism of *Proz-mediated PAR2*

activation is still unknown and a detailed investigation is required to delineate the molecular interaction. Furthermore, the functional characterization of lncRNA locus provides valuable insights into the diverse manifestations of development and disease processes. Large or small structural variants such as the 13q34 deletion syndrome can manifest with a range of symptoms, including developmental delays, intellectual disabilities, facial and cranial abnormalities, stroke, heart defects, and various other physical and medical issues. The absence of genes in this specific region of chromosome 13 can profoundly influence both the physical and intellectual development of individual humans affected by this syndrome. Our identified lncRNA locus, *scar-6*, is also located within the 13q34 region and its functional study demonstrates its involvement in hemostasis and the maintenance of endothelial barrier function and its loss of function can lead to stroke-like phenotype as observed in the case of 13q34 deletion syndrome. (Ponmani *et al*, 2015; Huang *et al*, 2012; Reinstein *et al*, 2016; Rath *et al*, 2015; Laurie & Bell, 2013).

These finding together highlights that the *scar-6* elncRNA locus is an important conserved regulatory locus in the organism that controls the expression of *prozb,* to maintain the normal levels of *coagulation factor Xa* in the organism and maintain proper homeostasis and vascular functioning in the organism.

Materials and Methods

In-silico selection of cardiovascular lncRNA and bioinformatics analysis

ZFLNC database was used in this study (Accessed Oct 1, 2018) (Hu *et al*, 2018). It contains a list of 13,604 lncRNA genes of zebrafish, obtained from RNA sequence data overlapped with Ensemble, NCBI, NONCODE, zflncRNApedia, and literature. All the lncRNA genomic

coordinates were downloaded from the ZFLNC database. Using the ZFLNC database, we curetted out the list of lncRNAs that were conserved between zebrafish and humans. In the database, 3 modes of conservation were used to identify the conserved lncRNA. For our study, we selected the syntenic and collinearity model of conservation and retained those lncRNA transcripts. The selected sets of lncRNA genes were further analyzed for their genomic location, size, and adjacent 5 neighboring genes using the genome map of the ZFLNC database. We downloaded a list of cardiovascular genes from Zfin using the terms heart, blood vessels, and endothelium cells. against the gene/transcript category individually(Bradford *et al*, 2022). The curated list of neighboring genes of lncRNAs was then overlapped individually with the list of cardiovascular genes. LncRNA with the overlapped neighboring genes were selected. Further, we prioritized the lncRNA genes having a single neighboring gene associated with any one of the selected tissues as they could be false-positive hits. In the end, we selected lncRNA which has more than 2 genes in synteny known to be functionally relevant in the cardiovascular system, their location, the importance of neighboring genes, disease association, and a number of human orthologs for further study.

We also computed the non-coding potential of the lncRNAs using bioinformatic algorithms such as the Coding Potential Assessment Tool (CPAT2) (Wang *et al*, 2013) or Coding Potential Calculator (CPC2)(Kang *et al*, 2017).

RNA-seq analysis was conducted as previously detailed (Ranjan *et al*, 2024) using publicly available datasets and reanalyzing them (Pauli *et al*, 2012; Yang *et al*, 2020; Sehgal *et al*, 2021).. The reads were aligned to the zebrafish danRer11 reference genome using STAR v2.7. Raw counts were obtained with htseq-count, and normalization was performed using DESeq2. Expression data were plotted using GraphPad v9. Transcription factor binding at the *scar-6* locus

was predicted using the JASPAR 2022 database (Castro-Mondragon *et al*, 2022) plugin track in the UCSC genome browser (Raney *et al*, 2024) for zebrafish danRer11 reference genome. Additionally, the UCSC genome browser (Raney *et al*, 2024) track for the zebrafish danRer10 genome was utilized to visualize genomic locations, repeat regions, and epigenetic marks (Danio-code data; (Raney *et al*, 2024; Baranasic *et al*, 2022).

RNA seqcondary structure was predicted using RNAfold web server (https://rna.tbi.univie.ac.at/cgi-bin/RNAWebSuite/RNAfold.cgi) (Lorenz *et al*, 2011) by using the RNA sequence of *scar-6* lncRNA and 12-bp edited *scar-6* lncRNA with default setting.

Animal study approval

The double transgenic zebrafish (*Danio rerio*) *gib004Tg(fli1a*:EGFP; *gata1a*:DsRed) (Lalwani *et al*, 2012; Lawson & Weinstein, 2002; Traver *et al*, 2003) and *scar-6*$^{gib007\Delta12/+}$ were maintained and handled in compliance with the protocols and guidelines approved by the Institutional Animal Ethics Committee of CSIR-Institute of Genomics and Integrative Biology, India (GENCODE-C-24). Special care was taken to ensure minimal distress to the animals.

Microinjection of CRISPR-Cas9 and IVT products into the embryo

We made a cocktail of 25ng/µl of sgRNA, 250ng/µl of Cas9 protein (Takara, Japan), and 200mM of KCl solution. The cocktail was preheated at 42°C for 5 min and then incubated in ice. The cocktail was loaded into the needle using a microloader tip. The needle was fixed into the Injection holder (Narishige, Japan) and the tip was calibrated accordingly to inject 3nl of the solution. Using the Harvard Apparatus pump (Harvard Apparatus, USA) 3nl of the cocktail was injected into the single-cell stage embryos which were loaded on the embryo loading plate and visualized under a Stereo microscope Zeiss (ZEISS, Germany). Double transgenic zebrafish *gib004Tg*(*fli1: EGFP; gata1a: dsRed*) embryos were used for injections (Lalwani *et al*, 2012;

Lawson & Weinstein, 2002; Traver *et al*, 2003). After the injection, the embryos were incubated at 28.5 °C in system water for 8 hpf and then transferred to embryo water (E3) containing 200 mM (0.003%) PTU (N- phenylthiourea, Sigma Aldrich) and further incubated at 28°C. The PTU embryo water was changed every 24 hrs and the dead and undeveloped embryos were removed simultaneously.

Similarly, *scar-6* ,*prozb* and *f10* were amplified from zebrafish cDNA and *in-vitro* transcribed using T7 mMESSAGE mMACHINE kit (Thermo Scientific), and different concentration was injected into the single cell stage of zebrafish as described above.

Microinjection of morpholino and dCas9-KRAB into the embryo

Antisense splice blocking morpholino oligonucleotide (MO) was designed to target the 2nd exon of *scar-6* (GeneTools, USA) (supplementary table 4). Morpholino was dissolved in nucleus-free water to a final stock concentration of 1mM. 3nl of different concentrations of MO was injected into 1 cell stage of double transgenic zebrafish *gib004Tg*(*fli1: EGFP; gata1a: dsRed*) and the phenotype was observed. Scrambled MO (CCTCTTACCTCAGTTACAATTTATA) was used for control injection.

Knockdown using dCas9-KRAB was performed as previously described (Long *et al*, 2015). We generated in vitro transcribed (IVT) RNA of the amplified dCas9-KRAB region from the Lenti-(BB)-EF1a-KRAB-dCas9-P2A-EGFP plasmid (a gift from Jorge Ferrer; Addgene plasmid #118156; http://n2t.net/addgene:118156; RRID) using the T7 mMessage mMachine kit. The sgRNA used in the knockout experiment was used. The injection was done at a final concentration of 300 ng/µl for dCas9-KRAB and 100 ng/µl for sgRNA. A single injection of dCas9-KRAB IVT was used as a control.

Heteroduplex mobility shift assay (HMA)

We used heteroduplex mobility assay (HMA) to identify indels in the mutant animals as described previously (Sehgal *et al*, 2021; Ota *et al*, 2013). We amplified the 230 bp region around the target size with denaturing and slow cooling at the end. The amplicon products were run on a non-denaturing 15% DNA PAGE gel and stained using EtBr to observe the mobility shift in the heterozygous mutants. To identify homozygous mutants, we spiked a wild-type amplicon product in the PCR reaction followed by denaturing and slow cooling and the product was similarly run on non-denaturing 15% DNA PAGE gel.

Mechanical Vascular Injury for Coagulation assay

We performed mechanical injury in the posterior cardinal vein (PCV) as described previously (Clay & Coughlin, 2015). Briefly, we anesthetize the 3dpf zebrafish embryos with 0.02% buffered 3-aminobenzoic acid (Tricaine). Using a minutia pin injury was made at the PVC of the zebrafish by piercing into it. The time for occlusion was recorded for up to 2 mins (120s) by a person who is blinded to the genotyping of the embryos. The individual embryos are genotyped after the assay is completed using HMA as described above.

RT-qPCR

RNA isolation was carried out using 15 embryos with TRIzol (Invitrogen) and phenol-chloroform, (Invitrogen). Subsequently, Turbo DNAse (Ambion) treatment and purification were conducted. cDNA was synthesized using 500 ng of total RNA and reverse transcriptase from Superscript II (Invitrogen). We used TB Green Premix Ex Taq II (Tli RNase H Plus) (TAKARA) to perform quantitative real-time PCR on LightCycler LC480 (Roche, Germany) or CFX384 BioRad. The relative levels of specific transcripts in the original pool of RNA were estimated using the methods described (Winer et al., 1999; Livak and Schmittgen,

2001). We used *actb* as a normalizing control for our analysis. The details for primers used for qRT-PCR are mentioned in the supplementary files.

Enhancer Assay

An enhancer assay was performed using E1b-GFP-Tol2 (a gift from Nadav Ahituv; Addgene plasmid # 37845 ; http://n2t.net/addgene:37845 ; RRID:Addgene_37845). The target region was amplified and inserted into the plasmid using BglII and XhoI restriction enzyme (NEB) upstream to the E1B promoter. The construct was confirmed using target-specific PCR and Sanger sequencing. We injected the zebrafish *scar-6* E1B-GFP and human *SCAR-6* E1B-GFP plasmid into the wild-type ASWT zebrafish (75 ng/ul) (Patowary *et al*, 2013). The zebrafish was monitored till 5 dpf and positive animals were grown till adult and outgrossed to develop the stable lines. The imaged accusation was done on an upright Zeiss Axioscope A1 fluorescent microscope (Carl Zeiss, Germany).

The psi-CHEK-2 plasmid (Promega) was used for the luciferase assay. The target region was amplified and cloned upstream of the SV40 promoter using BglII and Kpn1 restriction sites. HHL-17, HEK297T, HUVEC/hTert2, and HepG2 were transfected with the cloned vectors using lipofectamine 300 (Thermofisher), and enhancer activity was calculated by normalizing of renila luciferase signal with firefly luciferase signal.

Whole-mount *in-situ* hybridization (WISH)

With few modifications, WISH was performed according to a previously described protocol (Thisse & Thisse, 2008; Sehgal *et al*, 2021). Briefly, 3dpf or 5dpf embryos were fixed in 4% paraformaldehyde (PFA) at 4°C. The embryos were dehydrated and rehydrated using serial dilutions of methanol followed by proteinase K treatment. Hybridization of the DIG-UTP labeled RNA probe was performed overnight at 65° C and staining was performed using NBT/BCIP

(Sigma Aldrich) alkaline phosphatase substrates. Instead of PBST, we used tris-buffered saline and Tween 20 (1xTBST) buffer for stringent washing.

Subcellular RNA isolation

The subcellular isolation of zebrafish was performed as previously described with few modifications(Ten *et al*, 2012). Briefly, 500 embryos of 3dpf zebrafish were dissociated into single cells using 1x TrypLE Express (Gibco) and collagenase IV. The single cells were incubated and homogenized in hypotonic buffer (10mM HEPES, Ph 7.9; 1.5mM MgCl2; 10mM KCl; 0.5mM DTT;and Protease inhibitor) followed by centrifugation at 1000 rpm at 4°C for 5 min. The supernatant was collated as cytoplasm and the pellet was washed with hypotonic buffer and collected as a nucleus. 1 % of the sample was taken for western blotting and the rest was used for RNA isolation.

Evans blue dye injection

Evans blue dye injection was performed as previously described with slight modifications(Smith *et al*, 2015). Briefly, 1% Evans blue dye was made in 1X Ringers solution and 5 nl/embryos was injected in the common cardinal vein (CCV). The injected embryos was incubated for 3 hrs. Confocal microscopy was performed for the dye at 620 ex/ 680 em. 10 regions in intersegmental vessels of control and mutant was selected and the mean gray value was quantified using ImageJ from 3 independent animals.

ChIP-qPCR assay

The experiment was performed using the previously described method (Havis *et al*, 2006). Briefly, the pool of embryos (wt/*scar-6*$^{gib007\Delta12/\Delta12}$-20 embryos; scrMO/scar-6MO- 50 embryos) was fixed using formaldehyde and lysed using RIPA lysis buffer (Thermo scientific). The sample was sonicated using a sonicator with 10s on and 4 min off at 35% amplitude. The sample was centrifuged and incubated overnight in CTCF antibody (Abcam-ab70303) and was pulled using

protein A/G beads (Thermo Scientific) and purified using Qiagen PCR purification kit and quantified by qPCR. (primers in supplementary)

RIP-qRTPCR

The experiment was performed using the previously described method(Sehgal *et al*, 2021; Li *et al*, 2014). Briefly, 500 embryos of 3dpf zebrafish were lysed in RIPA buffer (Thermo scientific). The lysate was then UV crosslinked and then precleared in protein A/G beads. It was incubated with *IgG* (abcam-ab231712) *Suz12 (CST- ab3737)* and *prdm14 (abcam- ab187881)* antibodies overnight at 4℃. The antibody was pulled using magnetic protein A/G beads and was treated in PNK buffer (10mM NaCl, 10mM Tri-Cl pH7.6, 1mM EDTA, 0.5% SDS) and then mixed in Trizol and the RNA was extracted out. An equal concentration of RNA was used to prepare cDNA using SSRT II (Thermo scientific) and using TB Green Premix (Takara) qRT-PCR was performed.

Chromosome Conformation Capture (3C) assay

Chromosome Conformation Capture(3C) was performed as previously described with few modifications for zebrafish (Cope & Fraser, 2009). Briefly, the 20 embryos of 3dpf zebrafish were fixed using 1X formaldehyde and lysed using a cell lysis buffer (10 mM Tris-Cl (pH 8,1), 10 mM NaCl, 0.5% NP-40, proteinase inhibitors). The sample was digested using MseI restriction enzyme (NEB) overnight at 37℃, followed by ligation using T4 DNA ligase (NEB) overnight at 16℃. The DNA was isolated using phenol:chloroform:isoamyl alcohol (Invitrogen) method and the target region was quantified by qPCR. (primers in supplementary)

Targeted Bisulfite Sequencing

DNA was isolated for individual WT and *scar-6*$^{gib007\Delta12/\Delta12}$ zebrafish. Using Epi-Tech Bisulfite conversion kit (Qiagen) the DNA was treated following the instructions provided by the manual.

The targeted region was amplified and proceeded with amplicon sequencing on MiSeq. BS-Seq was used to align the reads to the zebrafish (danrer11) genome and methylation percentage was calculated (Hansen *et al*, 2012) .

DNA pulldown assay

Target *scar-6* locus was amplified using 5'biotin labeled forward primer using WT and *scar-6*$^{gib007\Delta12/\Delta12}$ DNA as templates. The PCR product was purified and incubated with magnetic steptavidin beads for 1 hr at room temperature then mixed with zebrafish lysate prepared from 500 embryos in RIPA lysis buffer (Thermo Scientific) and incubated overnight at 4℃. The next day the magnetic beads were pulled down and dissolved in the SDS buffer and heated for 20 min at 95℃ and then proceeded with immunoblotting with the prdm14 antibody.

Statistical analysis

All the statistical analysis was performed using GraphPad Prism v9 or R v4.0.

Western blotting

Western blot was performed as previously described. Briefly, the protein was isolated from zebrafish (NF-kβ p65 - 15 embryos; luciferase - 1 embryo) using NP-40 lysis buffer(Thermo Scientific) with protease inhibitor was run on 10% SDS-PAGE gel and transferred to the PVDF or nitrocellulose membrane. The primary antibody of NF-kβ p65 (CST-3033) was diluted to 1:1000 and the blot was incubated overnight with the primary antibody. HRP conjugated secondary antibody was diluted 1:10000 and incubated at room temperature and the blot was visualized using ECL under a chemiluminescence gel documentation system.

Cleavage assay

The firefly luciferase was amplified from psi-CHEK-2 plasmid (Promega), GFP was amplified from Lenti-(BB)-EF1a-KRAB-dCas9-P2A-EGFP plasmid(Addgene-118156) and PAR2 domain

was amplified from HEK 293T cDNA and all three was cloned in frame together using In-Fusion cloning(Takara) in the background of TOPO pCR2.1 vector(Thermo Scientific) to generated luciferase-PAR2 domain-GFP vector. The IVT of luciferase-PAR2 domain-GFP was made using T7 mMassage mMachine kit (Thermo Scientific) and 100 ng/ul was injected into single cell stage zebrafish (WT and *scar-6*$^{gib007\Delta12/\Delta12}$). At 3dpf the individual embryos were lysed using NP-40 lysis buffer (Thermo scientific) and western blotting was performed using Firefly luciferase (Thermo Scientific PA5-32209) at or 1:5000 dilution. HRP conjugated secondary antibody was diluted 1:10000 and incubated at room temperature and the blot was visualized using ECL under a chemiluminescence gel documentation system. Cleavge efficiency was calculated by the given formula.

Cleavage efficacy (%) = [luciferase intensity / Total (luciferase + luciferase-PAR2-GPF)] x 100

Data Availability

All the data has been provided in a supplementary file.

Funding

The funding for this work was provided by CSIR- MLP 2001

Conflict of Interest Disclosure

The author declares no conflict of interest.

Acknowledgments

The authors would like to acknowledge Samatha Mathews, for her input in designing experiments, discussions, and manuscript proofreading. We like to acknowledge Mercy Rophina and Arvind Kumar for their inputs in bioinformatics analysis. We acknowledge Hari Vignesh and Rahul Bhoyar for their help with sequencing. We also like to acknowledge Narendra Kumar for maintaining the zebrafish facility. We like to acknowledge Monika Verma, Dilip Kumar and Koushika Chandrasekaran for helping with the confocal microscope.. We like to acknowledge reagents from Debojyoti Chakraborty (CSIR-IGIB) for CTCF antibodies.

Author's contribution

GR, PS, VS, and SS conceived and designed the experiment, and GR performed the experiments and performed the bioinformatic analysis. GR, PS, VS, and SS analyzed the results. GR wrote the manuscript and GR, PS,VS, and SS edited the manuscript.

References

Alberelli MA & De Candia E (2014) Functional role of protease activated receptors in vascular biology. *Vascul Pharmacol* 62: 72–81

Allou L, Balzano S, Magg A, Quinodoz M, Royer-Bertrand B, Schöpflin R, Chan W-L, Speck-Martins CE, Carvalho DR, Farage L, *et al* (2021) Non-coding deletions identify Maenli lncRNA as a limb-specific En1 regulator. *Nature* 592: 93–98

Andergassen D, Muckenhuber M, Bammer PC, Kulinski TM, Theussl H-C, Shimizu T, Penninger JM, Pauler FM & Hudson QJ (2019) The Airn lncRNA does not require any DNA elements within its locus to silence distant imprinted genes. *PLoS Genet* 15: e1008268

Andersson R, Gebhard C, Miguel-Escalada I, Hoof I, Bornholdt J, Boyd M, Chen Y, Zhao X, Schmidl C, Suzuki T, *et al* (2014) An atlas of active enhancers across human cell types and tissues. *Nature* 507: 455–461

Anene-Nzelu CG, Lee MCJ, Tan WLW, Dashi A & Foo RSY (2021) Genomic enhancers in cardiac development and disease. *Nat Rev Cardiol* 19: 7–25

Arner E, Daub CO, Vitting-Seerup K, Andersson R, Lilje B, Drabløs F, Lennartsson A, Rönnerblad M, Hrydziuszko O, Vitezic M, *et al* (2015) Transcribed enhancers lead waves of coordinated transcription in transitioning mammalian cells. *Science* 347: 1010–1014

Bae J-S & Rezaie AR (2009) Thrombin inhibits nuclear factor kappaB and RhoA pathways in cytokine-stimulated vascular endothelial cells when EPCR is occupied by protein C. *Thromb Haemost* 101: 513–520

Baranasic D, Hörtenhuber M, Balwierz PJ, Zehnder T, Mukarram AK, Nepal C, Várnai C, Hadzhiev Y, Jimenez-Gonzalez A, Li N, *et al* (2022) Multiomic atlas with functional stratification and developmental dynamics of zebrafish cis-regulatory elements. *Nat Genet* 54: 1037–1050

Bedell VM, Person AD, Larson JD, McLoon A, Balciunas D, Clark KJ, Neff KI, Nelson KE, Bill BR, Schimmenti LA, *et al* (2012) The lineage-specific gene ponzr1 is essential for zebrafish pronephric and pharyngeal arch development. *Development* 139: 793–804

Bombeli T, Schwartz BR & Harlan JM (1998) Adhesion of activated platelets to endothelial cells: evidence for a GPIIbIIIa-dependent bridging mechanism and novel roles for endothelial intercellular adhesion molecule 1 (ICAM-1), alphavbeta3 integrin, and GPIbalpha. *J Exp Med* 187: 329–339

Bono F, Schaeffer P, Hérault JP, Michaux C, Nestor AL, Guillemot JC & Herbert JM (2000) Factor Xa activates endothelial cells by a receptor cascade between EPR-1 and PAR-2. *Arterioscler Thromb Vasc Biol* 20: E107–12

Bradford YM, Van Slyke CE, Ruzicka L, Singer A, Eagle A, Fashena D, Howe DG, Frazer K,

Martin R, Paddock H, *et al* (2022) Zebrafish information network, the knowledgebase for Danio rerio research. *Genetics* 220

Buddenkotte J, Stroh C, Engels IH, Moormann C, Shpacovitch VM, Seeliger S, Vergnolle N, Vestweber D, Luger TA, Schulze-Osthoff K, *et al* (2005) Agonists of proteinase-activated receptor-2 stimulate upregulation of intercellular cell adhesion molecule-1 in primary human keratinocytes via activation of NF-kappa B. *J Invest Dermatol* 124: 38–45

Byskov K, Etscheid M & Kanse SM (2020) Cellular effects of factor VII activating protease (FSAP). *Thromb Res* 188: 74–78

Cajigas I, Chakraborty A, Swyter KR, Luo H, Bastidas M, Nigro M, Morris ER, Chen S, VanGompel MJW, Leib D, *et al* (2018) The Evf2 Ultraconserved Enhancer lncRNA Functionally and Spatially Organizes Megabase Distant Genes in the Developing Forebrain. *Mol Cell* 71: 956–972.e9

Castro-Mondragon JA, Riudavets-Puig R, Rauluseviciute I, Lemma RB, Turchi L, Blanc-Mathieu R, Lucas J, Boddie P, Khan A, Manosalva Pérez N, *et al* (2022) JASPAR 2022: the 9th release of the open-access database of transcription factor binding profiles. *Nucleic Acids Res* 50: D165–D173

Cho SW, Xu J, Sun R, Mumbach MR, Carter AC, Chen YG, Yost KE, Kim J, He J, Nevins SA, *et al* (2018) Promoter of lncRNA Gene PVT1 Is a Tumor-Suppressor DNA Boundary Element. *Cell* 173: 1398–1412.e22

Ciliberti S, Martin OC & Wagner A (2007) Innovation and robustness in complex regulatory gene networks. *Proc Natl Acad Sci U S A* 104: 13591–13596

Clay H & Coughlin SR (2015) Mechanical vessel injury in zebrafish embryos. *J Vis Exp*: e52460

Cope NF & Fraser P (2009) Chromosome conformation capture. *Cold Spring Harb Protoc* 2009: db.prot5137

Cremer S, Michalik KM, Fischer A, Pfisterer L, Jaé N, Winter C, Boon RA, Muhly-Reinholz M, John D, Uchida S, *et al* (2019) Hematopoietic Deficiency of the Long Noncoding RNA MALAT1 Promotes Atherosclerosis and Plaque Inflammation. *Circulation* 139: 1320–1334

Cui J, O'Shea KS, Purkayastha A, Saunders TL & Ginsburg D (1996) Fatal haemorrhage and incomplete block to embryogenesis in mice lacking coagulation factor V. *Nature* 384: 66–68

Denis C, Methia N, Frenette PS, Rayburn H, Ullman-Culleré M, Hynes RO & Wagner DD (1998) A mouse model of severe von Willebrand disease: defects in hemostasis and thrombosis. *Proc Natl Acad Sci U S A* 95: 9524–9529

Dewerchin M, Liang Z, Moons L, Carmeliet P, Castellino FJ, Collen D & Rosen ED (2000) Blood coagulation factor X deficiency causes partial embryonic lethality and fatal neonatal bleeding in mice. *Thromb Haemost* 83: 185–190

Diederichs S (2014) The four dimensions of noncoding RNA conservation. *Trends Genet* 30: 121–123

Douglas AT & Hill RD (2014) Variation in vertebrate cis-regulatory elements in evolution and disease. *Transcription* 5: e28848

ENCODE Project Consortium, Moore JE, Purcaro MJ, Pratt HE, Epstein CB, Shoresh N, Adrian J, Kawli T, Davis CA, Dobin A, *et al* (2020) Expanded encyclopaedias of DNA elements in the human and mouse genomes. *Nature* 583: 699–710

van den Eshof BL, Hoogendijk AJ, Simpson PJ, van Alphen FPJ, Zanivan S, Mertens K, Meijer AB & van den Biggelaar M (2017) Paradigm of Biased PAR1 (Protease-Activated Receptor-1) Activation and Inhibition in Endothelial Cells Dissected by Phosphoproteomics. *Arterioscler Thromb Vasc Biol* 37: 1891–1902

Fatima R, Choudhury SR, T R D, Bhaduri U & Rao MRS (2019) A novel enhancer RNA, Hmrhl, positively regulates its host gene, in chronic myelogenous leukemia. *Noncoding RNA Res* 4: 96–108

Ferraro NM, Strober BJ, Einson J, Abell NS, Aguet F, Barbeira AN, Brandt M, Bucan M, Castel SE, Davis JR, *et al* (2020) Transcriptomic signatures across human tissues identify functional rare genetic variation. *Science* 369

Feyder M & Goff LA (2016) Investigating long noncoding RNAs using animal models. *J Clin Invest* 126: 2783–2791

Gil N, Perry RB-T, Mukamel Z, Tuck A, Bühler M & Ulitsky I (2023) Complex regulation of Eomes levels mediated through distinct functional features of the Meteor long non-coding RNA locus. *Cell Rep* 42: 112569

Gil N & Ulitsky I (2018) Production of Spliced Long Noncoding RNAs Specifies Regions with Increased Enhancer Activity. *Cell Syst* 7: 537–547.e3

Gil N & Ulitsky I (2020) Regulation of gene expression by cis-acting long non-coding RNAs. *Nat Rev Genet* 21: 102–117

Groff AF, Sanchez-Gomez DB, Soruco MML, Gerhardinger C, Barutcu AR, Li E, Elcavage L, Plana O, Sanchez LV, Lee JC, *et al* (2016) In Vivo Characterization of Linc-p21 Reveals Functional cis-Regulatory DNA Elements. *Cell Rep* 16: 2178–2186

Hansen KD, Langmead B & Irizarry RA (2012) BSmooth: from whole genome bisulfite sequencing reads to differentially methylated regions. *Genome Biol* 13: R83

Han X, Fiehler R & Broze GJ Jr (1998) Isolation of a protein Z-dependent plasma protease inhibitor. *Proc Natl Acad Sci U S A* 95: 9250–9255

Han X, Fiehler R & Broze GJ Jr (2000) Characterization of the protein Z-dependent protease inhibitor. *Blood* 96: 3049–3055

Han X, Luo S, Peng G, Lu JY, Cui G, Liu L, Yan P, Yin Y, Liu W, Wang R, *et al* (2018) Mouse knockout models reveal largely dispensable but context-dependent functions of lncRNAs during development. *J Mol Cell Biol* 10: 175–178

Havis E, Anselme I & Schneider-Maunoury S (2006) Whole embryo chromatin immunoprecipitation protocol for the in vivo study of zebrafish development. *Biotechniques* 40: 34, 36, 38 passim

Heinz S & Braspenning J (2015) Measurement of Blood Coagulation Factor Synthesis in Cultures of Human Hepatocytes. *Protocols in In Vitro Hepatocyte Research*: 309–316

Heuberger DM, Franchini AG, Madon J & Schuepbach RA (2019) Thrombin cleaves and activates the protease-activated receptor 2 dependent on thrombomodulin co-receptor availability. *Thromb Res* 177: 91–101

Heuberger DM & Schuepbach RA (2019) Protease-activated receptors (PARs): mechanisms of action and potential therapeutic modulators in PAR-driven inflammatory diseases. *Thromb J* 17: 1–24

Hezroni H, Koppstein D, Schwartz MG, Avrutin A, Bartel DP & Ulitsky I (2015) Principles of long noncoding RNA evolution derived from direct comparison of transcriptomes in 17 species. *Cell Rep* 11: 1110–1122

Hosono Y, Niknafs YS, Prensner JR, Iyer MK, Dhanasekaran SM, Mehra R, Pitchiaya S, Tien J, Escara-Wilke J, Poliakov A, *et al* (2017) Oncogenic Role of THOR, a Conserved Cancer/Testis Long Non-coding RNA. *Cell* 171: 1559–1572.e20

Hou Y, Zhang R & Sun X (2019) Enhancer LncRNAs Influence Chromatin Interactions in Different Ways. *Front Genet* 10: 936

Hsieh C-L, Fei T, Chen Y, Li T, Gao Y, Wang X, Sun T, Sweeney CJ, Lee G-SM, Chen S, *et al* (2014) Enhancer RNAs participate in androgen receptor-driven looping that selectively enhances gene activation. *Proc Natl Acad Sci U S A* 111: 7319–7324

Huang C, Yang Y-F, Yin N, Chen J-L, Wang J, Zhang H & Tan Z-P (2012) Congenital heart defect and mental retardation in a patient with a 13q33.1-34 deletion. *Gene* 498: 308–310 doi:10.1016/j.gene.2012.01.083 [PREPRINT]

Hu X, Chen W, Li J, Huang S, Xu X, Zhang X, Xiang S & Liu C (2018) ZFLNC: a comprehensive and well-annotated database for zebrafish lncRNA. *Database* 2018

Hu Z, Liu Y, Huarng MC, Menegatti M, Reyon D, Rost MS, Norris ZG, Richter CE, Stapleton AN, Chi NC, *et al* (2017) Genome editing of factor X in zebrafish reveals unexpected tolerance of severe defects in the common pathway. *Blood* 130: 666–676

Ishiguro K, Kojima T, Kadomatsu K, Nakayama Y, Takagi A, Suzuki M, Takeda N, Ito M, Yamamoto K, Matsushita T, *et al* (2000) Complete antithrombin deficiency in mice results in embryonic lethality. *J Clin Invest* 106: 873–878

Ishii N, Ozaki K, Sato H, Mizuno H, Susumu Saito, Takahashi A, Miyamoto Y, Ikegawa S, Kamatani N, Hori M, *et al* (2006) Identification of a novel non-coding RNA, MIAT, that confers risk of myocardial infarction. *J Hum Genet* 51: 1087–1099

Islam Z, Saravanan B, Walavalkar K, Farooq U, Singh AK, Radhakrishnan S, Thakur J, Pandit A, Henikoff S & Notani D (2023) Active enhancers strengthen insulation by RNA-mediated CTCF binding at chromatin domain boundaries. *Genome Res* 33: 1–17

Ivaldi MS, Diaz LF, Chakalova L, Lee J, Krivega I & Dean A (2018) Fetal γ-globin genes are regulated by the long noncoding RNA locus. *Blood* 132: 1963–1973

Jacobs J, Pagani M, Wenzl C & Stark A (2023) Widespread regulatory specificities between transcriptional co-repressors and enhancers in. *Science* 381: 198–204

Jalbert LR, Rosen ED, Moons L, Chan JC, Carmeliet P, Collen D & Castellino FJ (1998) Inactivation of the gene for anticoagulant protein C causes lethal perinatal consumptive coagulopathy in mice. *J Clin Invest* 102: 1481–1488

Kang Y-J, Yang D-C, Kong L, Hou M, Meng Y-Q, Wei L & Gao G (2017) CPC2: a fast and accurate coding potential calculator based on sequence intrinsic features. *Nucleic Acids Res* 45: W12–W16

Katsushima K, Joshi K, Yuan M, Romero B, Batish M, Stapleton S, Jallo G, Kolanthai E, Seal S, Saulnier O, *et al* (2024) A therapeutically targetable positive feedback loop between lnc-HLX-2-7, HLX, and MYC that promotes group 3 medulloblastoma. *Cell Rep* 43: 113938

Kemkes-Matthes B & Matthes KJ (1995) Protein Z, a new haemostatic factor, in liver diseases. *Haemostasis* 25: 312–316

Koch F, Fenouil R, Gut M, Cauchy P, Albert TK, Zacarias-Cabeza J, Spicuglia S, de la Chapelle AL, Heidemann M, Hintermair C, *et al* (2011) Transcription initiation platforms and GTF recruitment at tissue-specific enhancers and promoters. *Nat Struct Mol Biol* 18: 956–963

Kopp F & Mendell JT (2018) Functional Classification and Experimental Dissection of Long Noncoding RNAs. *Cell* 172: 393–407

Kurian L, Aguirre A & Sancho-Martinez I (2016) Identification of Novel Long Noncoding RNAs Underlying Vertebrate Cardiovascular Development. *Journal of Vascular Surgery* 63: 280–281 doi:10.1016/j.jvs.2015.11.008 [PREPRINT]

Lalwani MK, Sharma M, Singh AR, Chauhan RK, Patowary A, Singh N, Scaria V & Sivasubbu S (2012) Reverse genetics screen in zebrafish identifies a role of miR-142a-3p in vascular development and integrity. *PLoS One* 7: e52588

Lam MTY, Li W, Rosenfeld MG & Glass CK (2014) Enhancer RNAs and regulated transcriptional programs. *Trends Biochem Sci* 39: 170–182

Laurie AD & Bell J-A (2013) Severe FX deficiency caused by a homozygous double deletion involving F10 and PROZ genes. *Haemophilia* 19: e361–4

Lawson ND & Weinstein BM (2002) In vivo imaging of embryonic vascular development using transgenic zebrafish. *Dev Biol* 248: 307–318

Lee J-H, Wang R, Xiong F, Krakowiak J, Liao Z, Nguyen PT, Moroz-Omori EV, Shao J, Zhu X, Bolt MJ, *et al* (2021) Enhancer RNA m6A methylation facilitates transcriptional condensate formation and gene activation. *Mol Cell* 81: 3368–3385.e9

Leisegang MS, Fork C, Josipovic I, Richter FM, Preussner J, Hu J, Miller MJ, Epah J, Hofmann P, Günther S, *et al* (2017) Long Noncoding RNA MANTIS Facilitates Endothelial Angiogenic Function. *Circulation* 136: 65–79

Lewandowski JP, Dumbović G, Watson AR, Hwang T, Jacobs-Palmer E, Chang N, Much C, Turner KM, Kirby C, Rubinstein ND, *et al* (2020) The Tug1 lncRNA locus is essential for male fertility. *Genome Biol* 21: 237

Li K, Blum Y, Verma A, Liu Z, Pramanik K, Leigh NR, Chun CZ, Samant GV, Zhao B, Garnaas MK, *et al* (2010) A noncoding antisense RNA in tie-1 locus regulates tie-1 function in vivo. *Blood* 115: 133–139

Liu Y, Kretz CA, Maeder ML, Richter CE, Tsao P, Vo AH, Huarng MC, Rode T, Hu Z, Mehra R, *et al* (2014) Targeted mutagenesis of zebrafish antithrombin III triggers disseminated intravascular coagulation and thrombosis, revealing insight into function. *Blood* 124: 142–150

Li W, Notani D, Ma Q, Tanasa B, Nunez E, Chen AY, Merkurjev D, Zhang J, Ohgi K, Song X, *et al* (2013) Functional roles of enhancer RNAs for oestrogen-dependent transcriptional activation. *Nature* 498: 516–520

Li W, Notani D & Rosenfeld MG (2016) Enhancers as non-coding RNA transcription units: recent insights and future perspectives. *Nat Rev Genet* 17: 207–223

Li X, Lu Y-C, Dai K, Torregroza I, Hla T & Evans T (2014) Elavl1a regulates zebrafish erythropoiesis via posttranscriptional control of gata1. *Blood* 123: 1384–1392

Li X, Wang J, Jiang Z, Guo F, Soloway PD & Zhao R (2015) Role of PRDM16 and its PR domain in the epigenetic regulation of myogenic and adipogenic genes during transdifferentiation of C2C12 cells. *Gene* 570: 191–198

Loeffen R, Spronk HMH & ten Cate H (2012) The impact of blood coagulability on atherosclerosis and cardiovascular disease. *J Thromb Haemost* 10: 1207–1216

Long L, Guo H, Yao D, Xiong K, Li Y, Liu P, Zhu Z & Liu D (2015) Regulation of transcriptionally active genes via the catalytically inactive Cas9 in C. elegans and D. rerio. *Cell Res* 25: 638–641

Lorenz R, Bernhart SH, Höner Zu Siederdissen C, Tafer H, Flamm C, Stadler PF & Hofacker IL (2011) ViennaRNA Package 2.0. *Algorithms Mol Biol* 6: 26

Lowe CB, Kellis M, Siepel A, Raney BJ, Clamp M, Salama SR, Kingsley DM, Lindblad-Toh K & Haussler D (2011) Three periods of regulatory innovation during vertebrate evolution. *Science* 333: 1019–1024

Marsman RF, Tan HL & Bezzina CR (2013) Genetics of sudden cardiac death caused by ventricular arrhythmias. *Nat Rev Cardiol* 11: 96–111

Mathew S & Sivasubbu S (2022) Long Non Coding RNA Based Regulation of Cerebrovascular Endothelium. *Front Genet* 13: 834367

Mattick JS, Amaral PP, Carninci P, Carpenter S, Chang HY, Chen L-L, Chen R, Dean C, Dinger ME, Fitzgerald KA, *et al* (2023) Long non-coding RNAs: definitions, functions, challenges and recommendations. *Nat Rev Mol Cell Biol* 24: 430–447

McEwen GK, Goode DK, Parker HJ, Woolfe A, Callaway H & Elgar G (2009) Early evolution of conserved regulatory sequences associated with development in vertebrates. *PLoS Genet* 5: e1000762

Minami T, Abid MR, Zhang J, King G, Kodama T & Aird WC (2003) Thrombin stimulation of vascular adhesion molecule-1 in endothelial cells is mediated by protein kinase C (PKC)-delta-NF-kappa B and PKC-zeta-GATA signaling pathways. *J Biol Chem* 278: 6976–6984

Minami T, Sugiyama A, Wu S-Q, Abid R, Kodama T & Aird WC (2004) Thrombin and phenotypic modulation of the endothelium. *Arterioscler Thromb Vasc Biol* 24: 41–53

Modzelewski AJ, Gan Chong J, Wang T & He L (2022) Mammalian genome innovation through transposon domestication. *Nat Cell Biol* 24: 1332–1340

Nakashima Y, Raines EW, Plump AS, Breslow JL & Ross R (1998) Upregulation of VCAM-1 and ICAM-1 at atherosclerosis-prone sites on the endothelium in the ApoE-deficient mouse. *Arterioscler Thromb Vasc Biol* 18: 842–851

Natoli G & Andrau J-C (2012) Noncoding transcription at enhancers: general principles and functional models. *Annu Rev Genet* 46: 1–19

Neumann P, Jaé N, Knau A, Glaser SF, Fouani Y, Rossbach O, Krüger M, John D, Bindereif A, Grote P, *et al* (2018) The lncRNA GATA6-AS epigenetically regulates endothelial gene expression via interaction with LOXL2. *Nat Commun* 9: 237

Oksuz O, Henninger JE, Warneford-Thomson R, Zheng MM, Erb H, Vancura A, Overholt KJ, Hawken SW, Banani SF, Lauman R, *et al* (2023) Transcription factors interact with RNA to regulate genes. *Mol Cell*

Oo JA, Brandes RP & Leisegang MS (2022) Long non-coding RNAs: novel regulators of

cellular physiology and function. *Pflugers Arch* 474: 191–204

Ørom UA, Derrien T, Beringer M, Gumireddy K, Gardini A, Bussotti G, Lai F, Zytnicki M, Notredame C, Huang Q, *et al* (2010) Long noncoding RNAs with enhancer-like function in human cells. *Cell* 143: 46–58

Ota S, Hisano Y, Muraki M, Hoshijima K, Dahlem TJ, Grunwald DJ, Okada Y & Kawahara A (2013) Efficient identification of TALEN-mediated genome modifications using heteroduplex mobility assays. *Genes Cells* 18: 450–458

Paralkar VR, Taborda CC, Huang P, Yao Y, Kossenkov AV, Prasad R, Luan J, Davies JOJ, Hughes JR, Hardison RC, *et al* (2016) Unlinking an lncRNA from Its Associated cis Element. *Mol Cell* 62: 104–110

Park C, Kim TM & Malik AB (2013) Transcriptional Regulation of Endothelial Cell and Vascular Development. *Circ Res*

Patowary A, Purkanti R, Singh M, Chauhan R, Singh AR, Swarnkar M, Singh N, Pandey V, Torroja C, Clark MD, *et al* (2013) A sequence-based variation map of zebrafish. *Zebrafish* 10: 15–20

Pauli A, Valen E, Lin MF, Garber M, Vastenhouw NL, Levin JZ, Fan L, Sandelin A, Rinn JL, Regev A, *et al* (2012) Systematic identification of long noncoding RNAs expressed during zebrafish embryogenesis. *Genome Res* 22: 577–591

Payer B, Rosenberg M, Yamaji M, Yabuta Y, Koyanagi-Aoi M, Hayashi K, Yamanaka S, Saitou M & Lee JT (2013) Tsix RNA and the germline factor, PRDM14, link X reactivation and stem cell reprogramming. *Mol Cell* 52: 805–818

Pérez-Rico YA, Barillot E & Shkumatava A (2020) Demarcation of Topologically Associating Domains Is Uncoupled from Enriched CTCF Binding in Developing Zebrafish. *iScience* 23: 101046

Pnueli L, Rudnizky S, Yosefzon Y & Melamed P (2015) RNA transcribed from a distal enhancer is required for activating the chromatin at the promoter of the gonadotropin α-subunit gene. *Proc Natl Acad Sci U S A* 112: 4369–4374

Ponmani C, Giri D, Hussain K & Senniappan S (2015) 13q Deletion in a Girl Contributing to Antenatal Stroke, Insulin Resistance and Lymphedema Praecox: Expanding the Clinical Spectrum. *Journal of Medical Cases* 6: 264–267 doi:10.14740/jmc2108w [PREPRINT]

Rabiet MJ, Plantier JL, Rival Y, Genoux Y, Lampugnani MG & Dejana E (1996) Thrombin-induced increase in endothelial permeability is associated with changes in cell-to-cell junction organization. *Arterioscler Thromb Vasc Biol* 16: 488–496

Ramos AD, Andersen RE, Liu SJ, Nowakowski TJ, Hong SJ, Gertz C, Salinas RD, Zarabi H, Kriegstein AR & Lim DA (2015) The long noncoding RNA Pnky regulates neuronal differentiation of embryonic and postnatal neural stem cells. *Cell Stem Cell* 16: 439–447

Raney BJ, Barber GP, Benet-Pagès A, Casper J, Clawson H, Cline MS, Diekhans M, Fischer C, Navarro Gonzalez J, Hickey G, *et al* (2024) The UCSC Genome Browser database: 2024 update. *Nucleic Acids Res* 52: D1082–D1088

Ranjan G, Scaria V & Sivasubbu S (2024) Syntenic lncRNAs exhibit DNA regulatory functions with sequence evolution. *bioRxiv*: 2024.04.26.588027

Ranjan G, Sehgal P, Sharma D, Scaria V & Sivasubbu S (2021) Functional long non-coding and circular RNAs in zebrafish. *Brief Funct Genomics*

Rath M, Najm J, Sirb H, Kentouche K, Dufke A, Pauli S, Hackmann K, Liehr T, Hübner CA, Felbor U, *et al* (2015) Large deletions play a minor but essential role in congenital coagulation factor VII and X deficiencies. *Hamostaseologie* 35 Suppl 1: S36–42

Reinstein E, Liberman M, Feingold-Zadok M, Tenne T & Graham JM Jr (2016) Terminal microdeletions of 13q34 chromosome region in patients with intellectual disability: Delineation of an emerging new microdeletion syndrome. *Mol Genet Metab* 118: 60–63

Ritter N, Ali T, Kopitchinski N, Schuster P, Beisaw A, Hendrix DA, Schulz MH, Müller-McNicoll M, Dimmeler S & Grote P (2019) The lncRNA Locus Handsdown Regulates Cardiac Gene Programs and Is Essential for Early Mouse Development. *Dev Cell* 50: 644–657.e8

Roadmap Epigenomics Consortium, Kundaje A, Meuleman W, Ernst J, Bilenky M, Yen A, Heravi-Moussavi A, Kheradpour P, Zhang Z, Wang J, *et al* (2015) Integrative analysis of 111 reference human epigenomes. *Nature* 518: 317–330

Rom A, Melamed L, Gil N, Goldrich MJ, Kadir R, Golan M, Biton I, Perry RB-T & Ulitsky I (2019) Regulation of CHD2 expression by the Chaserr long noncoding RNA gene is essential for viability. *Nat Commun* 10: 5092

Santoro F, Mayer D, Klement RM, Warczok KE, Stukalov A, Barlow DP & Pauler FM (2013) Imprinted Igf2r silencing depends on continuous Airn lncRNA expression and is not restricted to a developmental window. *Development* 140: 1184–1195

Sarangdhar MA, Chaubey D, Bhatt A, Km M, Kumar M, Ranjan S & Pillai B (2017) A Novel Long Non-coding RNA, Modulates Dendrite Density and Expression of in Zebrafish. *Front Mol Neurosci* 10: 95

Sato M, Kadomatsu T, Miyata K, Warren JS, Tian Z, Zhu S, Horiguchi H, Makaju A, Bakhtina A, Morinaga J, *et al* (2021) The lncRNA Caren antagonizes heart failure by inactivating DNA damage response and activating mitochondrial biogenesis. *Nat Commun* 12: 2529

Sauvageau M, Goff LA, Lodato S, Bonev B, Groff AF, Gerhardinger C, Sanchez-Gomez DB, Hacisuleyman E, Li E, Spence M, *et al* (2013) Multiple knockout mouse models reveal lincRNAs are required for life and brain development. *Elife* 2: e01749

Schertzer MD, Braceros KCA, Starmer J, Cherney RE, Lee DM, Salazar G, Justice M, Bischoff

SR, Cowley DO, Ariel P, *et al* (2019) lncRNA-Induced Spread of Polycomb Controlled by Genome Architecture, RNA Abundance, and CpG Island DNA. *Mol Cell* 75: 523–537.e10

Sehgal P, Mathew S, Sivadas A, Ray A, Tanwar J, Vishwakarma S, Ranjan G, Shamsudheen KV, Bhoyar RC, Pateria A, *et al* (2021) LncRNA VEAL2 regulates PRKCB2 to modulate endothelial permeability in diabetic retinopathy. *EMBO J* 40: e107134

Sejima H, Hayashi T, Deyashiki Y, Nishioka J & Suzuki K (1990) Primary structure of vitamin K-dependent human protein Z. *Biochem Biophys Res Commun* 171: 661–668

Shapiro JA (2014) Constraint and opportunity in genome innovation. *RNA Biol* 11: 186–196

Sigova AA, Abraham BJ, Ji X, Molinie B, Hannett NM, Guo YE, Jangi M, Giallourakis CC, Sharp PA & Young RA (2015) Transcription factor trapping by RNA in gene regulatory elements. *Science* 350: 978–981

Smith SJ, Horstick EJ, Davidson AE & Dowling J (2015) Analysis of Zebrafish Larvae Skeletal Muscle Integrity with Evans Blue Dye. *J Vis Exp*

Sofi F, Cesari F, Fedi S, Abbate R & Gensini GF (2004) Protein Z: 'light and shade' of a new thrombotic factor. *Clin Lab* 50: 647–652

Spielmann N, Miller G, Oprea TI, Hsu C-W, Fobo G, Frishman G, Montrone C, Haseli Mashhadi H, Mason J, Munoz Fuentes V, *et al* (2022) Extensive identification of genes involved in congenital and structural heart disorders and cardiomyopathy. *Nature Cardiovascular Research* 1: 157–173

Srivastava D & Olson EN (2000) A genetic blueprint for cardiac development. *Nature* 407: 221–226

Sriwai W, Mahavadi S, Al-Shboul O, Grider JR & Murthy KS (2013) Distinctive G Protein-Dependent Signaling by Protease-Activated Receptor 2 (PAR2) in Smooth Muscle: Feedback Inhibition of RhoA by cAMP-Independent PKA. *PLoS One* 8: e66743

Statello L, Fernandez-Justel JM, González J, Montes M, Ranieri A, Goñi E, Mas AM & Huarte M (2024) The chromatin-associated lncREST ensures effective replication stress response by promoting the assembly of fork signaling factors. *Nat Commun* 15: 978

Staton J, Sayer M, Hankey GJ, Cole V, Thom J & Eikelboom JW (2005) Protein Z gene polymorphisms, protein Z concentrations, and ischemic stroke. *Stroke* 36: 1123–1127

St Laurent G, Wahlestedt C & Kapranov P (2015) The Landscape of long noncoding RNA classification. *Trends Genet* 31: 239–251

Sun J, Li W, Sun Y, Yu D, Wen X, Wang H, Cui J, Wang G, Hoffman AR & Hu J-F (2014) A novel antisense long noncoding RNA within the IGF1R gene locus is imprinted in hematopoietic malignancies. *Nucleic Acids Res* 42: 9588–9601

Sun L, Gai J, Shi S, Zhao J, Bai X, Liu B & Li X (2021) Protease-Activated Receptor 2 (PAR-2) Antagonist AZ3451 Mitigates Oxidized Low-Density Lipoprotein (Ox-LDL)-Induced Damage and Endothelial Inflammation. *Chem Res Toxicol* 34: 2202–2208

Tan JY & Marques AC (2022) The activity of human enhancers is modulated by the splicing of their associated lncRNAs. *PLoS Comput Biol* 18: e1009722

Ten S, Hodge K & I. A (2012) Dynamic proteomics: Methodologies and analysis. In *Functional Genomics* InTech

Thisse C & Thisse B (2008) High-resolution in situ hybridization to whole-mount zebrafish embryos. *Nat Protoc* 3: 59–69

Traver D, Paw BH, Poss KD, Penberthy WT, Lin S & Zon LI (2003) Transplantation and in vivo imaging of multilineage engraftment in zebrafish bloodless mutants. *Nat Immunol* 4: 1238–1246

Trimm E & Red-Horse K (2022) Vascular endothelial cell development and diversity. *Nat Rev Cardiol* 20: 197–210

Ulitsky I, Shkumatava A, Jan CH, Sive H & Bartel DP (2011) Conserved function of lincRNAs in vertebrate embryonic development despite rapid sequence evolution. *Cell* 147: 1537–1550

Viré E, Brenner C, Deplus R, Blanchon L, Fraga M, Didelot C, Morey L, Van Eynde A, Bernard D, Vanderwinden J-M, *et al* (2006) The Polycomb group protein EZH2 directly controls DNA methylation. *Nature* 439: 871–874

Vollmers AC, Covarrubias S, Kuang D, Shulkin A, Iwuagwu J, Katzman S, Song R, Viswanathan K, Vollmers C, Wakeland E, *et al* (2021) A conserved long noncoding RNA, GAPLINC, modulates the immune response during endotoxic shock. *Proc Natl Acad Sci U S A* 118

Walpola PL, Gotlieb AI, Cybulsky MI & Langille BL (1995) Expression of ICAM-1 and VCAM-1 and monocyte adherence in arteries exposed to altered shear stress. *Arterioscler Thromb Vasc Biol* 15: 2–10

Wang KC, Yang YW, Liu B, Sanyal A, Corces-Zimmerman R, Chen Y, Lajoie BR, Protacio A, Flynn RA, Gupta RA, *et al* (2011) A long noncoding RNA maintains active chromatin to coordinate homeotic gene expression. *Nature* 472: 120–124

Wang L, Park HJ, Dasari S, Wang S, Kocher J-P & Li W (2013) CPAT: Coding-Potential Assessment Tool using an alignment-free logistic regression model. *Nucleic Acids Res* 41: e74

Wang Y, Song F, Zhang B, Zhang L, Xu J, Kuang D, Li D, Choudhary MNK, Li Y, Hu M, *et al* (2018) The 3D Genome Browser: a web-based browser for visualizing 3D genome organization and long-range chromatin interactions. *Genome Biol* 19: 151

Wei N, Pang W, Wang Y, Xiong Y, Xu R, Wu W, Zhao C & Yang G (2014) Knockdown of PU.1 mRNA and AS lncRNA regulates expression of immune-related genes in zebrafish Danio rerio. *Dev Comp Immunol* 44: 315–319

Weyand AC, Grzegorski SJ, Rost MS, Lavik KI, Ferguson AC, Menegatti M, Richter CE, Asselta R, Duga S, Peyvandi F, *et al* (2019) Analysis of factor V in zebrafish demonstrates minimal levels needed for early hemostasis. *Blood Adv* 3: 1670–1680

Willis Fox O & Preston RJS (2020) Molecular basis of protease-activated receptor 1 signaling diversity. *J Thromb Haemost* 18: 6–16

Wu M, Zhang S, Chen X, Xu H & Li X (2019) Expression and function of lncRNA MALAT-1 in the embryonic development of zebrafish. *Gene* 680: 65–71

Yamaji M, Ueda J, Hayashi K, Ohta H, Yabuta Y, Kurimoto K, Nakato R, Yamada Y, Shirahige K & Saitou M (2013) PRDM14 ensures naive pluripotency through dual regulation of signaling and epigenetic pathways in mouse embryonic stem cells. *Cell Stem Cell* 12: 368–382

Yang H, Luan Y, Liu T, Lee HJ, Fang L, Wang Y, Wang X, Zhang B, Jin Q, Ang KC, *et al* (2020) A map of cis-regulatory elements and 3D genome structures in zebrafish. *Nature* 588: 337–343

Yin Y, Yan P, Lu J, Song G, Zhu Y, Li Z, Zhao Y, Shen B, Huang X, Zhu H, *et al* (2015) Opposing Roles for the lncRNA Haunt and Its Genomic Locus in Regulating HOXA Gene Activation during Embryonic Stem Cell Differentiation. *Cell Stem Cell* 16: 504–516

Zhang L, Segal AZ, Leifer D, Silverstein RL, Gerber LM, Devereux RB & Kizer JR (2017) Circulating protein Z concentration, PROZ variants, and unexplained cerebral infarction in young and middle-aged adults. *Thromb Haemost* 117: 149–157

Zhang Z, Lee J-H, Ruan H, Ye Y, Krakowiak J, Hu Q, Xiang Y, Gong J, Zhou B, Wang L, *et al* (2019) Transcriptional landscape and clinical utility of enhancer RNAs for eRNA-targeted therapy in cancer. *Nat Commun* 10: 4562

Zhao JV & Schooling CM (2018) Coagulation Factors and the Risk of Ischemic Heart Disease: A Mendelian Randomization Study. *Circ Genom Precis Med* 11: e001956

Figure legends

Figure 1: *Syntenic cardiovascular conserved associated region - 6 (scar-6)* is a novel conserved lncRNA gene

[A] Schematic of pipeline used for subset selection of syntenic lncRNAs with its neighboring protein-coding genes associated in the cardiovascular system. Overview of conserved syntenic block depiction of *scar-6* locus between human and zebrafish.

[B-C] UCSC genome browser snapshot of *scar-6* locus in zebrafish and human. Strand-specific PCR and 3'RACE confirmed the transcript to be antisense to f10 in zebrafish.

[D] Expression profile of *scar-6* transcript (in TPM) across 8 different developmental stages of zebrafish using publically available RNA-seq data.

[E] Expression profile of *scar-6* transcript (in TPM) across 12 different tissues using publically available RNA-seq data.

[F] Whole mount in-situ hybridization expression analysis of *scar-6, f10,* and *prozb* transcripts of zebrafish in 3dpf embryo. Sense probes were used as controls for *f10* and *prozb.* No probe control was used for *scar-6.*

Figure 2: - *scar-6*$^{gib007\Delta12/\Delta12}$ mutant exhibits permeability defect with haemorrhage phenotype.

[A] CRISPR-Cas9 mediated editing of *scar-6* locus at exon 2 resulting in a stable 12-bp deletion zebrafish line named *scar-6*$^{gib007\Delta12}$.

[B] Chromatogram representing the sequence of wildtype and homozygous mutant of *scar-6*$^{gib007\Delta12}$

[C] Schematic representing in-cross of *scar-6*$^{gib007\Delta12/+}$ zebrafish.

[D]Pie chart representing mutation segregation of the progeny from in-cross of *scar-6*$^{gib007\Delta12/+}$ zebrafish. The genotype of the progeny followed the Mendelian ratio.

[E] Box plot representing the percentage of animals from the in-cross of *scar-6*$^{gib007\Delta12/+}$ zebrafish exhibiting haemorrhage phenotype compared to wild-type control animals. Data from 3 independent in-cross of *scar-6*$^{gib007\Delta12/+}$ zebrafish plotted min to max with line at mean value ; ** p=0.0023 (two-tailed unpaired t-test).

[F]Representative image showing the cranial region of 3dpf zebrafish wild-type gib004Tg(*fli1a:*EGFP;*gata1a*:DsRed) and *scar-6*$^{gib007\Delta12/\Delta12}$ zebrafish (40x resolution)

[G]Bar plot representation of hemorrhage phenotype associated with genotyped *scar-6*$^{gib007\Delta12/+}$ in-crossed zebrafish animals. Data from 3 independent in-cross of *scar-6*$^{gib007\Delta12/+}$ zebrafish experiment plotted as mean percentage.

[H]Representative image showing intersegmental vessels (ISV) of 3 dpf wild-type and *scar-6*$^{gib007\Delta12/\Delta12}$ zebrafish injected with evans blue dye.

[I]Quantitative analysis of vascular permeability in wild-type and *scar-6*$^{gib007\Delta12/\Delta12}$ zebrafish injected with Evans blue dye. Data of 10 different ROI from 4 individual zebrafish from each wild-type and *scar-6*$^{gib007\Delta12/\Delta12}$ zebrafish plotted as mean ± standard deviation; **** p-value ≤ 0.0001.(Mann-Whitney U).

[J]Bar plot representing relative fold change in expression levels of *f10, scar-6* and *prozb* between wild-type and *scar-6*$^{gib007\Delta12/\Delta12}$ zebrafish. The *prozb* expression levels were 8-fold increase in the *scar-6*$^{gib007\Delta12/\Delta12}$ zebrafish compared to the wild-type. Data from 3 independent biological replicates plotted as mean fold change ± standard deviation; *** p-value ≤ 0.001 (unpaired two-tail t-test)

Figure 3:- The *scar-6* locus exhibits a functional role in the hemostatic process

[A] Coagulation assay plot calculating the time of occlusion (s) in different individual zebrafish in control and progeny of in-cross *scar-6*$^{gib007\Delta12/+}$ zebrafish performed blinded of the genotype of the animals. Combined data from 3 independent experiments with each point representing the occlusion time of individual zebrafish segregated based on genotype: **** p<0.0001 (Mann-Whitney U).

[B] Coagulation assay plot calculating the time of occlusion (s) in different individual zebrafish in control and different concentration of *scar-6* IVT (100, 200, 500 ng/ul) injected embryos performed blinded of the injected concentration. Combined data from 3 independent experiments with each point representing the occlusion time of individual zebrafish segregated based on injected concentration; **** p<0.0001 (Mann-Whitney U)

[C] Survival curve representing survival percentage of closely monitored control and *scar-6*$^{gib007\Delta12/\Delta12}$ zebrafish. p<0.0001 (log-rank test)

[D, E]Representative image at 30 dpf zebrafish of control and *scar-6*$^{gib007\Delta12/\Delta12}$ group closely monitored for survival. The red arrowhead indicates haemorrhage and cranial edema in *scar-6*$^{gib007\Delta12/\Delta12}$ mutant animals.

[F]Coagulation assay plot calculating the time of occlusion (s) in different individual zebrafish in control, in-cross progeny of *scar-6*$^{gib007\Delta12/+}$, in-cross progeny of *scar-6*$^{gib007\Delta12/+}$ injected with WT *scar-6* IVT RNA(100ng/ul) and in-cross progeny of *scar-6*$^{gib007\Delta12/+}$ injected with *scar-6*$^{gib007\Delta12}$ IVT RNA(100ng/ul) performed blinded. Each point representing the occlusion time of individual zebrafish segregated based on injected concentration; ns- not significant ** $p<0.01$ **** $p<0.0001$ (Mann-Whitney U)

[G]Representative image of the cranial region of zebrafish at 3dpf of control wild-type, in-cross progeny of *scar-6*$^{gib007\Delta12/+}$ and in-cross progeny of *scar-6*$^{gib007\Delta12/+}$ injected with WT *scar-6* IVT RNA(100ng/ul). The arrowhead indicates haemorrhage in the animals.

[H] Box plot representing the percentage of animals from control wild-type, in-cross of *scar-6*$^{gib007\Delta12/+}$ zebrafish and , in-cross of *scar-6*$^{gib007\Delta12/+}$ + *scar-6* IVT RNA (100ng/ul) exhibiting haemorrhage phenotype. Data from 3 experiments plotted min to max with line at mean value ; ns- not significant (two-tailed unpaired t-test).

[I]Relative fold change expression of *scar-6, f10,* and *prozb* when compared between control wild-type, *scar-6*$^{gib007\Delta12/\Delta12}$ animals and *scar-6*$^{gib007\Delta12/\Delta12}$ + *scar-6* IVT RNA (100ng/ul) animals. Data from 3 independent biological replicates plotted as mean fold change ± standard deviation; ns- not significant; ** $P<0.01$ (two-tailed unpaired t-test)

Figure 4: The *scar-6* locus exhibits cis-regulatory enhancer signature.

[A] UCSC genome browser snapshot of zebrafish *scar-6* locus with chromatin annotation marks from danio-code data across 5 developmental stages.

[B] UCSC genome browser snapshot of human *SCAR-6* locus with regulatory signature track from ENCODE data, chromatin annotation of 8 different cell lines from Epigenome roadmap project and enhancer data from GeneHancer database.

[C] Representative image of enhancer assay for human and zebrafish *scar-6* locus in zebrafish injected with empty E1b-GFP, *scar-6*-E1b-GFP and human *SCAR-6*-E1b-GFP. Transient expression was observed in the F_0 animals in the cardiac region and in case of human *SCAR-6* some expression was also observed in the trunk region.

[D] Bar plot of luciferase enhancer assay for human and zebrafish *scar-6* locus in HHL-17; HEK297T ; HUVEC/hTERT; and HepG2 cell line transfected with zebrafish *scar-6*-psi-Chek2 and human *SCAR-6*-psi-Chek2 plasmid. Enhancer function was observed in HUVEC/hTERT;

and HepG2 cell line. Data from 3 independent biological replicates plotted as mean fold change ± standard deviation; ns- not significant, * P<0.05, ** P<0.01, **** p<0.0001 (two-tailed unpaired t-test).

[E] Representative image of 3C experimental for *scar-6* and *prozb* locus and bar plot representing relative fold change between wild type and *scar-6*$^{gib007\Delta12/\Delta12}$ mutant zebrafish normalized with actb. The *scar-6*$^{gib007\Delta12/\Delta12}$ zebrafish showed an increase in the *scar-6/prozb* looping. Data from 3 independent biological replicates plotted as mean fold change ± SEM.* P<0.05 (two-tailed unpaired t-test).

Figure 5: The *scar-6* elncRNA gene epigentically regulates expression of *prozb* via *prdm14-PRC2* complex.

[A] UCSC genome browser screenshot representing JASPER 2022 track with 12 bp deletion of *scar-6* locus.

[B]Bar plot representing ChIP-qPCR quantification in percentage input using *prdm14* antibody as a target and mock as a control for *scar-6* locus in wild type and *scar-6*$^{gib007\Delta12/\Delta12}$ mutant zebrafish. Data from 3 independent biological replicates plotted as mean fold change ± standard deviation; ns- not significant, * P<0.05 (two-tailed unpaired t-test).

[C]Box and whiskers plot representing percentage methylation profile of proximal CpG island of *scar-6* using targeted bisulfite sequencing of wild type and *scar-6*$^{gib007\Delta12/\Delta12}$ mutant zebrafish per cytosine. Data from 4 independent biological replicates plotted with line at mean.

[D] Bar plot representing fold enrichment of *scar-6* elncRNA upon RNA-immunoprecipitation of *prdm14* and *Suz12* followed by qPCR of *scar-6* elncRNA. The *scar-6* elncRNA shows enrichment in the binding with *prdm14* and *Suz12*. Data from 3 independent biological replicates plotted as mean fold change ± standard deviation;* P<0.05, ** P<0.01(two-tailed unpaired t-test).

[E]Bar plot representing ChIP-qPCR quantification in percentage input using *prdm14* antibody as a target and mock as a control for *scar-6* locus in zebrafish injected with *scar-6* elncRNA morpholino (*scar-6* MO) and scrambled morpholino (scr MO). Data from 3 independent biological replicates plotted as mean fold change ± standard deviation; ** P<0.01, *** P<0.001, **** p<0.0001 (two-tailed unpaired t-test).

[F]Schematic representation of *prdm14-PCR-2* complex binding at *scar-6* locus and being

stabalized by the *scar-6* elncRNA produced from the *scar-6* elncRNA gene.

Figure 6:- *Prozb* mediated endothelial cells activation via the PAR2-NF-kb pathway in *scar-6*$^{gib007\Delta12/\Delta12}$ mutants,

[A] Representative image showing fluorescence for blood (*gata1a:DsRed)* in the cranial region of 3dpf zebrafish and o-dianisidine stating of RBC blood cells in control and *prozb* IVT RNA (80ng/ul) injected zebrafish.

[B]Stacked bar plot representing the phenotypic percentage of animals with haemorrhage and trunk deformities observed in control and *prozb* IVT RNA (80ng/ul) injected zebrafish. Data from 3 independent biological replicates plotted as mean percentage ± standard deviation.

[C] Bar plot representing relative fold change in expression of different PAR receptors (PAR1, PAR2a/b and PAR3) when compared between wild type and *scar-6*$^{gib007\Delta12/\Delta12}$ mutant zebrafish. The PAR2a/b receptors expression levels were ~2 fold upregulated in *scar-6*$^{gib007\Delta12/\Delta12}$ mutant zebrafish. Data from 3 independent biological replicates plotted as mean fold change ± standard deviation; ns- not significant, ** P<0.01, **** p<0.0001 (two-tailed unpaired t-test).

[D]Schematic representation of *in-vivo* PAR2 protease assay performed using eGFP-PAR2 domain-luciferase construct upon injecting into wild type and *scar-6*$^{gib007\Delta12/\Delta12}$ mutant zebrafish followed by western blotting with luciferase antibody. The bar plot represents the quantification of cleavage activity in the wild type and *scar-6*$^{gib007\Delta12/\Delta12}$ mutant zebrafish using the immunoblot quantification data. Data from 3 independent biological replicates plotted as mean ± standard deviation; ** P<0.01(two-tailed unpaired t-test)

[E]Western blot of NF-kB in wild type and *scar-6*$^{gib007\Delta12/\Delta12}$ mutant zebrafish. The bar plot represents the quantification of the western blot from 3 independent biological replicates plotted as mean fold change ± standard deviation.* P<0.05 (two-tailed unpaired t-test)

[F]Bar plot representing relative fold change expression of *vcam1a, vcam1b, icam1, inos2a*, and *inos2b* when compared between wild type and *scar-6*$^{gib007\Delta12/\Delta12}$ mutant zebrafish. Data from 3 independent biological replicates plotted as mean fold change ± standard deviation; ns- not significant, * P<0.05, ** P<0.01(two-tailed unpaired t-test).

[G] Hypothetical schematic of *prozb* mediated endothelial cell activation through activation of *PAR2-NF-κB* pathway leading to upregulation of surface adhesion molecules (*Icam1* and *Vcam1*) and downregulation of *iNOS2a* causing vascular dysfunction and haemorrhage in zebrafish.

Figure 7- Epigenetic regulation of *prozb* through *scar-6* locus is important for vascular function and hemostatic process.

Hypothetical schematic of *scar-6* locus in wild-type zebrafish, where *scar-6 elncRNA* and *prdm14 -PRC2* complex hypermethylated the proximal CpG island and inhibits CTCF binding. In *scar-6*$^{gib007\Delta12/\Delta12}$ mutant zebrafish. The 12 bp deletion affects the binding of the *scar-6 elncRNA* and *prdm14 -PRC2* complex leading to a partial change in methylation. This change allows the CTCF occupancy at the locus further mediating sub-TAD looping of the enhancer-promoter of *prozb*. This causes upregulation of *prozb* leading to endothelial cell activation via the PAR2-NF-κB pathway and causing vascular dysfunction leading to hemorrhage

Evidence figure legends

Figure EV1: - *scar-6* lncRNA transcript is ubiquitously expressed and nuclear enriched.

[A] Image showing agarose gel electrophoresis of the PCR product derived from *scar-6* lncRNA and *β-actin*, amplified from cDNA synthesized using both oligo dT(dT) and random hexamer primers (RH).

[B]Coding potentiality scores were calculated using CPC2 for *scar-6* and other lncRNA and protein-coding genes (*f10 and prozb*).

[C] Western blot of *HSP90*, *β-actin* and H4 histone to confirm the purity of sub-cellular fractions of zebrafish cells.

[D] The bar plot represents the relative abundance of the of *scar-6, f10* and *prozb* in different subcellular fractions quantified using qRT-PCR. The *scar-6* and *prozb* exhibit enrichment in the nucleus fraction and *f10* shows equal enrichment in cytoplasm and nucleus. Data from 3 different experiments plotted as relative abundance percentages ± SEM.

[E] Expression profile of human *SCAR-6* lncRNA across different tissues in GTEx v8 database.

Figure EV2:- CRISPR-Cas9 mediated mutant generation of *scar-6* lncRNA gene.

[A]DNA-PAGE gel illustrating the results of the heteroduplex mobility assay (HMA) conducted on the *scar-6* targeted region in F_1 *scar-6* mutant adult zebrafish, with genotypes identified by in-dels. Extra bands in the PAGE gel represents heteroduplex templates formed due to hetrozygosity in the target region.

[B] Representative image showing blood vessels of 3dpf zebrafish progeny derived from wild-type gib004Tg(*fli1a:*EGFP;*gata1a*:DsRed) and *scar-6*$^{gib007\Delta12/\Delta12}$ zebrafish.

Figure EV3: - Knockdown of *scar-6* shows no significant phenotype.

[A] Schematic of antisense splice blocking morpholino oligo targeting the exon 1 splicing junction of *scar-6* lncRNA.

[B] Relative fold change expression of *scar-6* upon of knockdown with splice blocking morpholino in zebrafish at 3dpf. Data from 3 independent biological replicates plotted as mean fold change ± standard deviation; * P<0.05 (two-tailed unpaired t-test)

[C] Floating bar plot representing the percentage of animals with haemorrhage phenotype in zebrafish embryos injected with 250uM of morpholino. Data from 3 experiments plotted min to max with line at mean value; ns- not significant (two-tailed unpaired t-test).

[D]Representative image of gib004Tg(*fli1a:*EGFP;*gata1a*:DsRed) zebrafish injected with different concentration of morpholino at 3 dpf (2.5x magnification).

[E]Relative fold change expression of *f10* and *prozb* upon knockdown of *scar-6* lncRNA with splice blocking morpholino in zebrafish. Data from 3 independent biological replicates plotted as mean fold change ± standard deviation; ns- not significant (two-tailed unpaired t-test)

[F]Coagulation assay plot calculating the time of occlusion (s) in different individual zebrafish in control and 500uM morpholino injected zebrafish. Each point represents the occlusion time of individual zebrafish segregated based on genotype; * P<0.05 (Mann-Whitney U).

Figure EV4: CRISPRi of *scar-6* locus exhibits haemorrhage phenotype

[A]Representation of CRISPR-dCas9-KRAB mediated inhibition of TF binding on *scar-6* locus.

[B]Representative image showing fluorescence for blood (*gata1a:DsRed)* in the cranial region of 3dpf zebrafish and o-dianisidine stating of RBC blood cells in control and dCas-9-KRAB + sg*scar-6* injected zebrafish.(4x magnification)

[C]Box plot representing the percentage of animals exhibiting haemorrhage phenotype in control and dCas-9-KRAB + sg*scar-6* injected zebrafish. Data from 3 independent biological replicates plotted as mean fold change ± standard deviation;* P<0.05 (two-tailed unpaired t-test).

Figure EV5: Sub-TAD looping mediated enhancer-promoter interaction of *scar-6/prozb*

locus

[A]Hi-C heatmap representation of Human *SCAR-6* locus in HepG2 at 10kb resolution from ENCODE database (ENCODE Project Consortium *et al*, 2020; Wang *et al*, 2018) and zebrafish *scar-6* locus in brain tissue at 5kb resolution from (Yang *et al,* 2020).

[B]UCSC genome browser snapshot of data for CTCF binding peaks at 24 hpf of zebrafish for at *scar-6* and *prozb* locus (Pérez-Rico *et al,* 2020).

[C]Bar plot representing ChIP-qPCR quantifying fold enrichment using CTCF antibody for *scar-6* locus in wild type and *scar-6*$^{gib007\Delta12/\Delta12}$ mutant zebrafish. Data from 3 independent biological replicates plotted as mean fold enrichment ± standard deviation; * $P<0.05$, ** $P<0.01$ (two-tailed unpaired t-test).

[D]Schematic and western blot of DNA-pulldown assay performed using streptavidin tagged *scar-6* gene DNA in zebrafish and immuno blotting using *prdm14* antibody. N=3

Figure 1

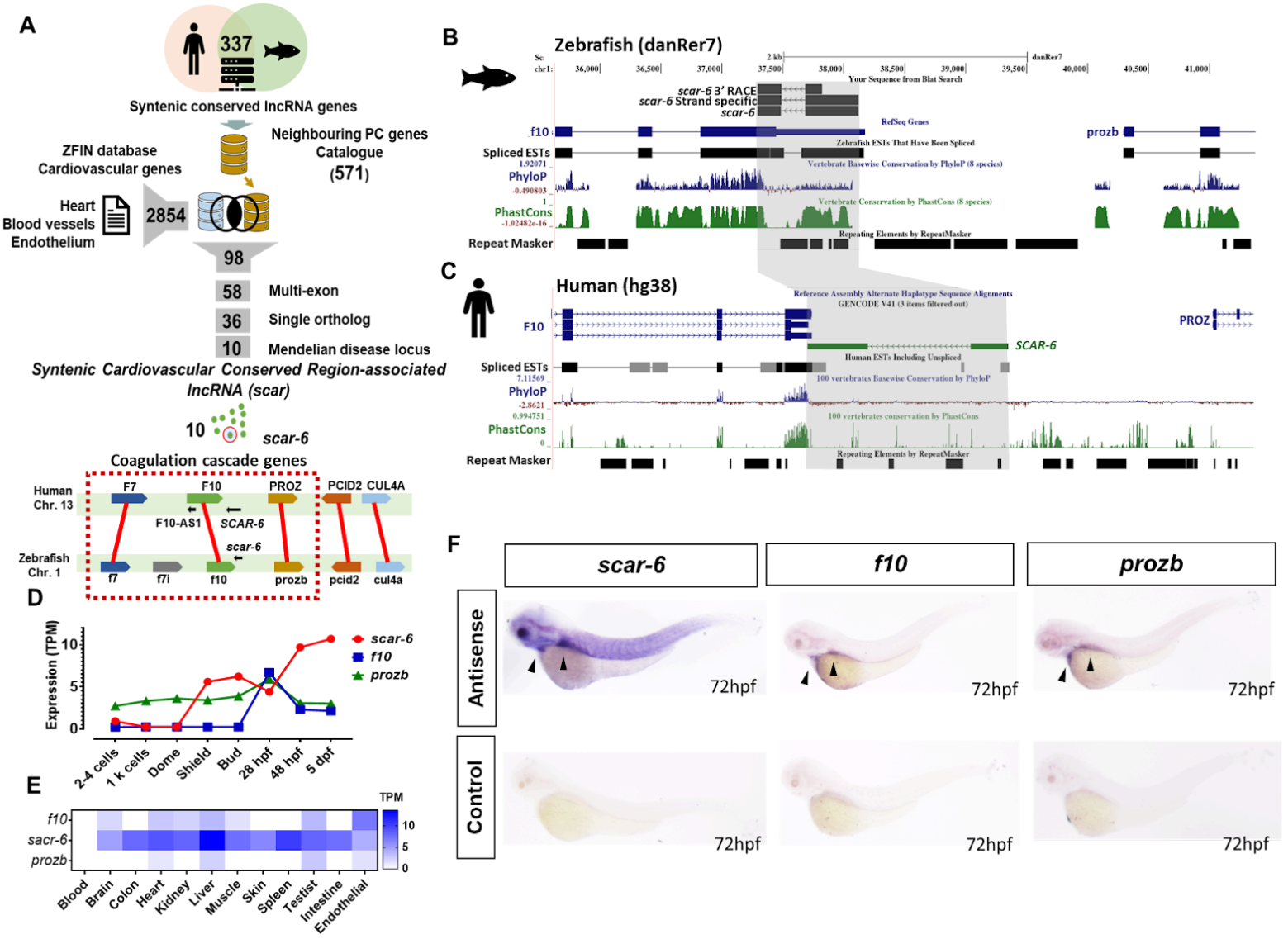
A
337
Syntenic conserved lncRNA genes
ZFIN database
Cardiovascular genes
Neighbouring PC genes
Catalogue
(571)
Heart
Blood vessels
Endothelium
2854
98
58 Multi-exon
36 Single ortholog
10 Mendelian disease locus
Syntenic Cardiovascular Conserved Region-associated lncRNA (scar)
10
scar-6
Coagulation cascade genes
Human Chr. 13
F7
F10
PROZ
PCID2
CUL4A
F10-AS1
SCAR-6
scar-6
Zebrafish Chr. 1
f7
f7i
f10
prozb
pcid2
cul4a
B
Zebrafish (danRer7)
scar-6 3' RACE
scar-6 Strand specific
scar-6
f10
prozb
Spliced ESTs
PhyloP
PhastCons
Repeat Masker
C
Human (hg38)
F10
PROZ
SCAR-6
Spliced ESTs
PhyloP
PhastCons
Repeat Masker
D
Expression (TPM)
scar-6
f10
prozb
2-4 cells
1 k cells
Dome
Shield
Bud
28 hpf
48 hpf
5 dpf
E
TPM
f10
sacr-6
prozb
Blood
Brain
Colon
Heart
Kidney
Liver
Muscle
Skin
Spleen
Testist
Intestine
Endothelial
F
scar-6
f10
prozb
Antisense
Control
72hpf

Figure 2

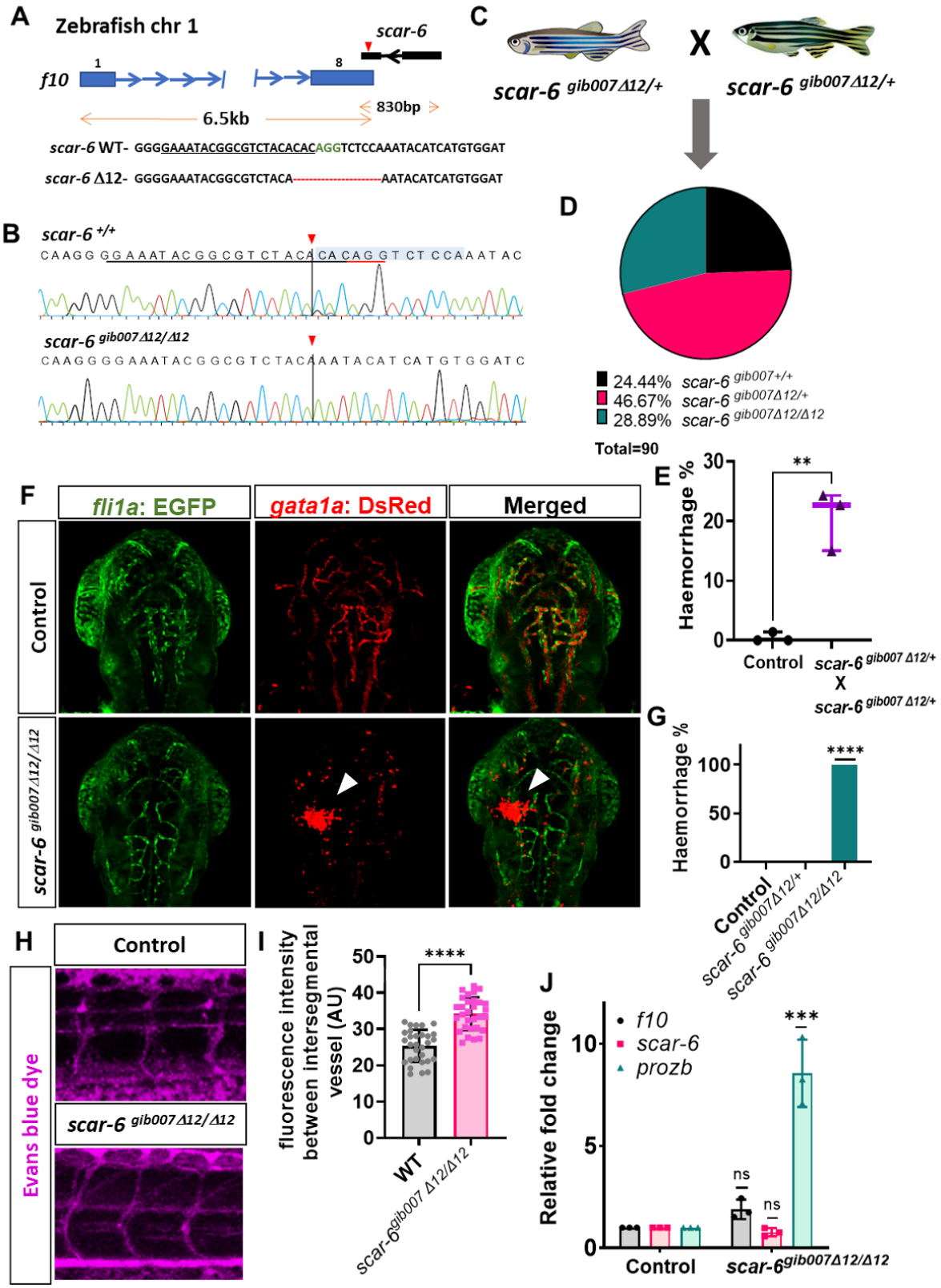

Figure 3

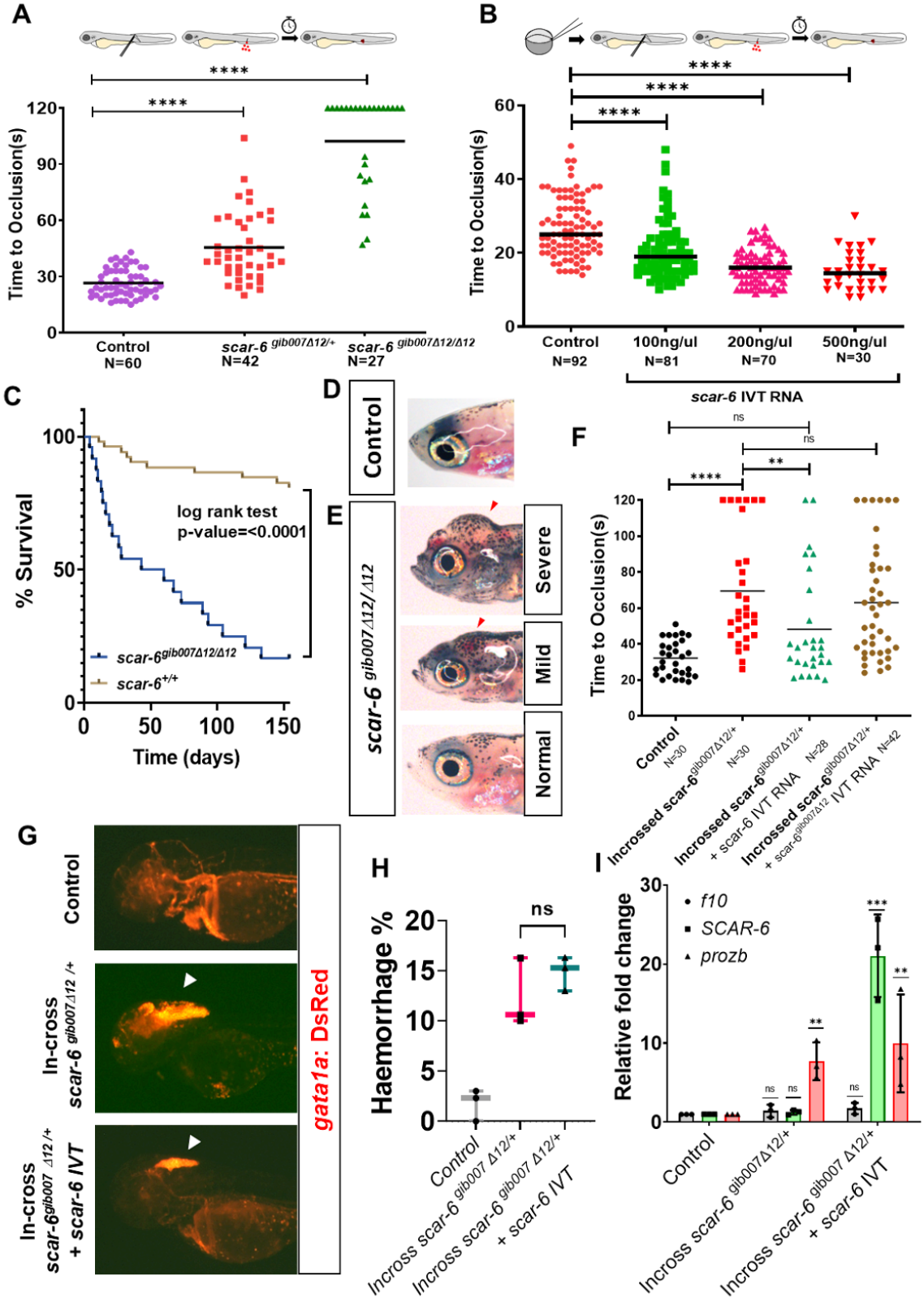

Figure 4

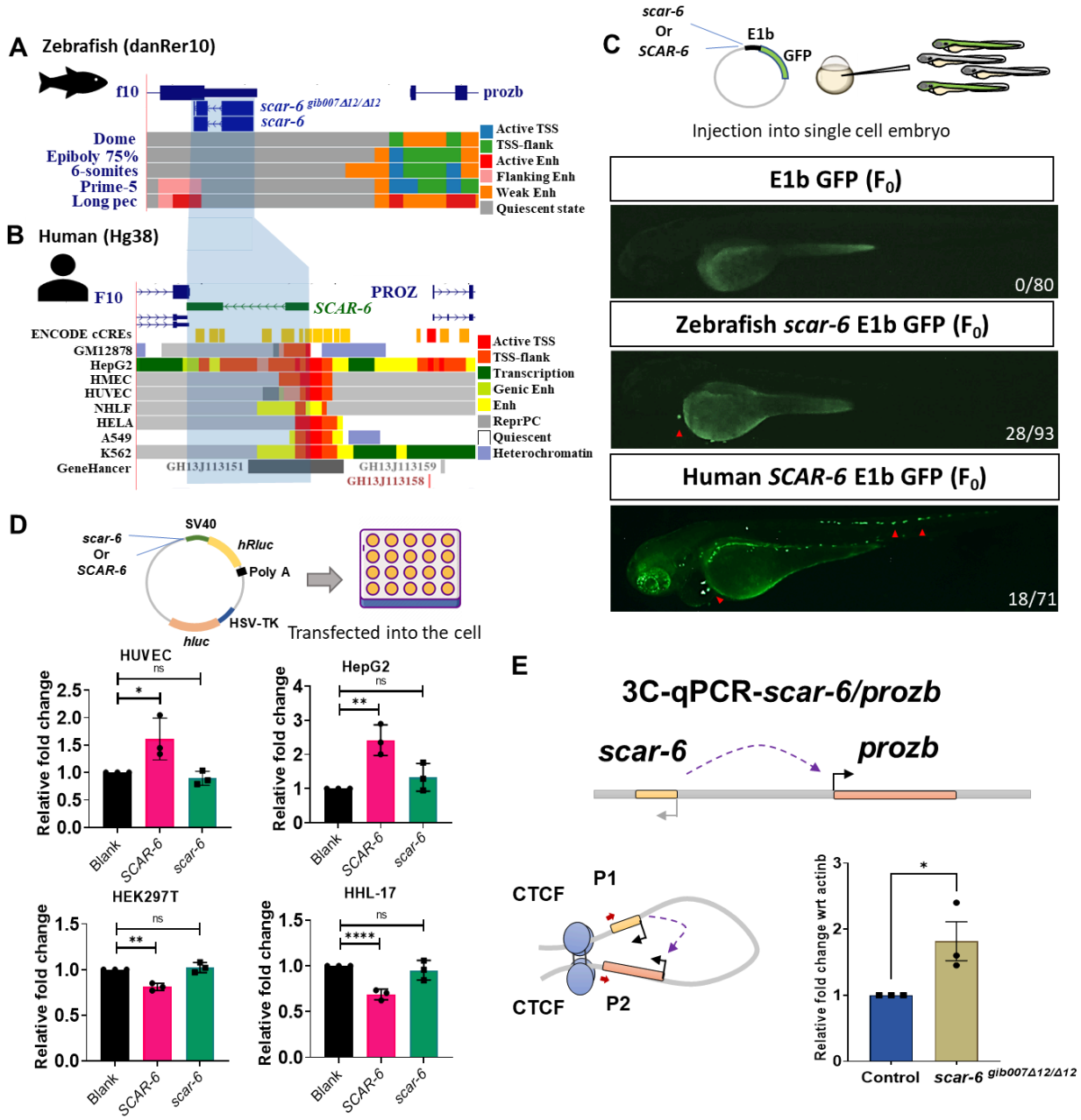

Figure 5

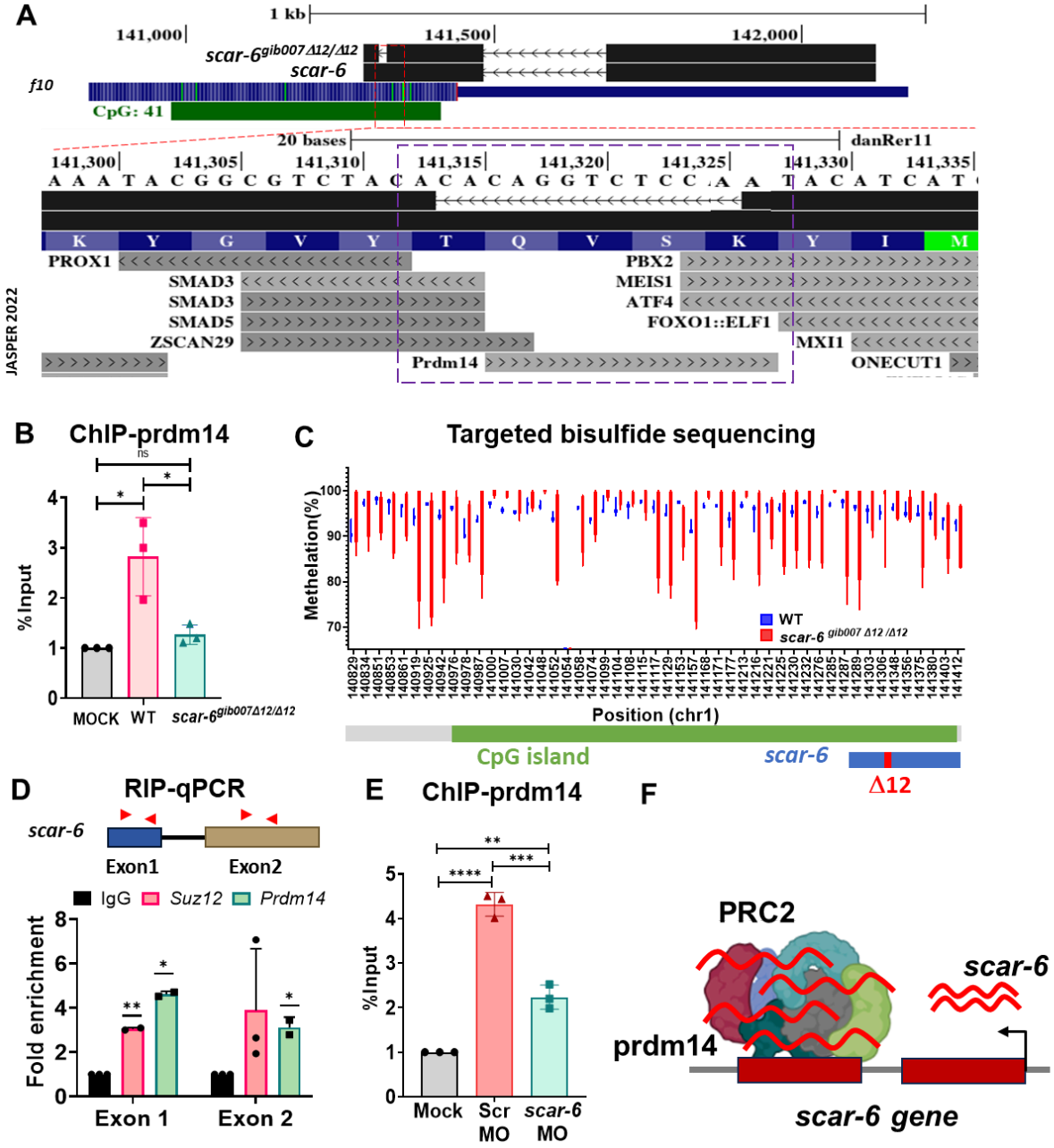

Figure 6

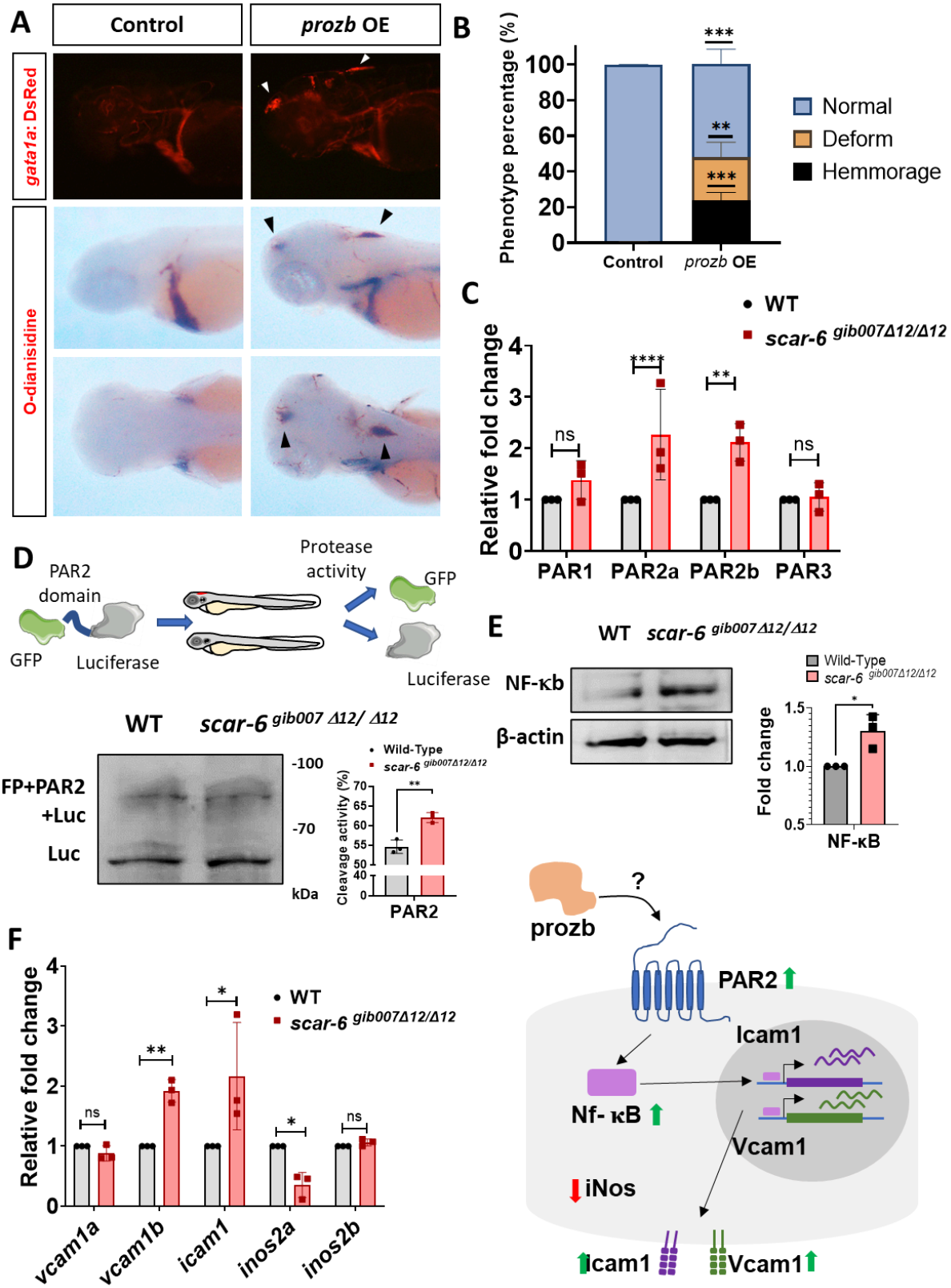

Figure 7

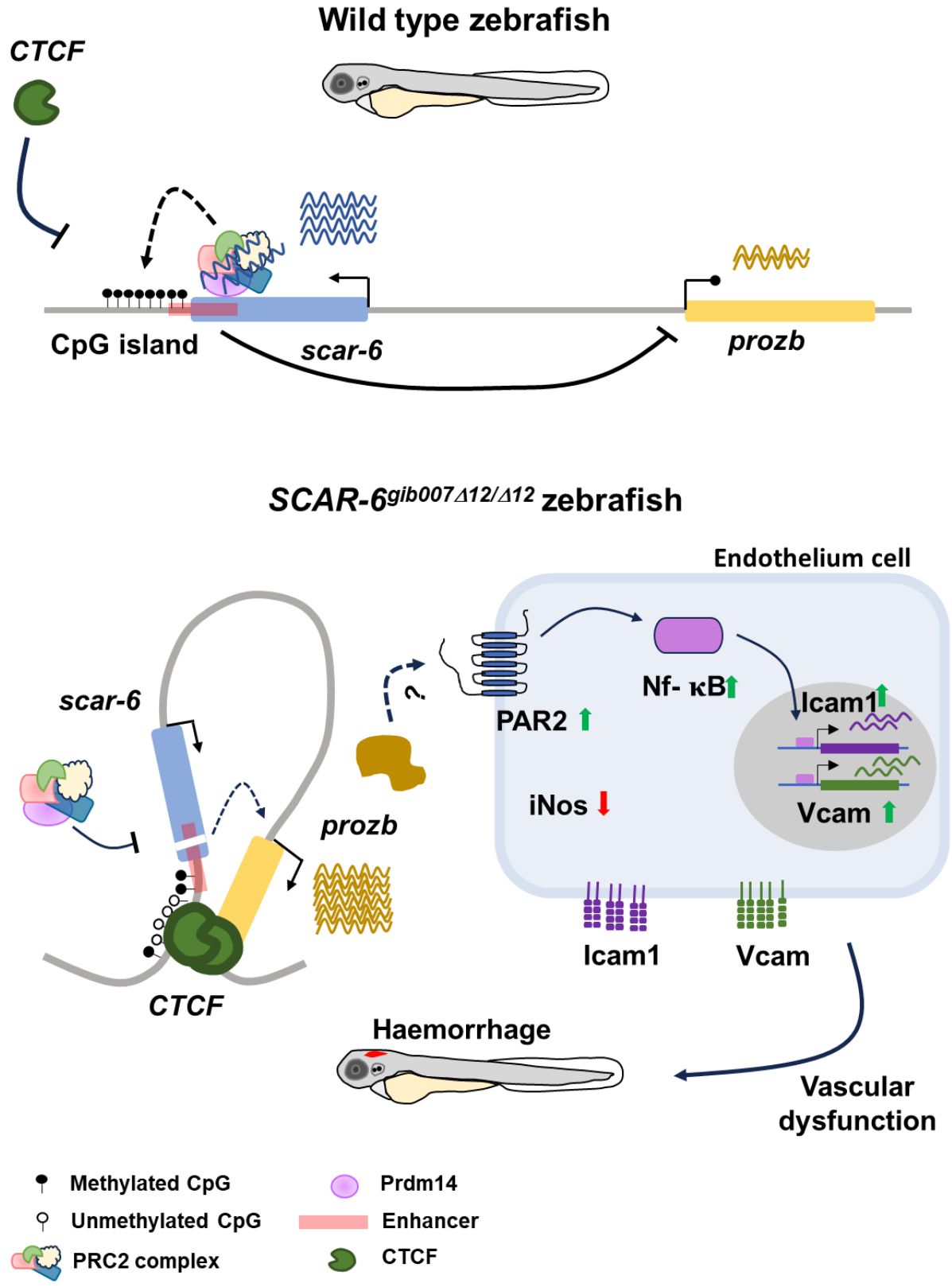

Figure EV1

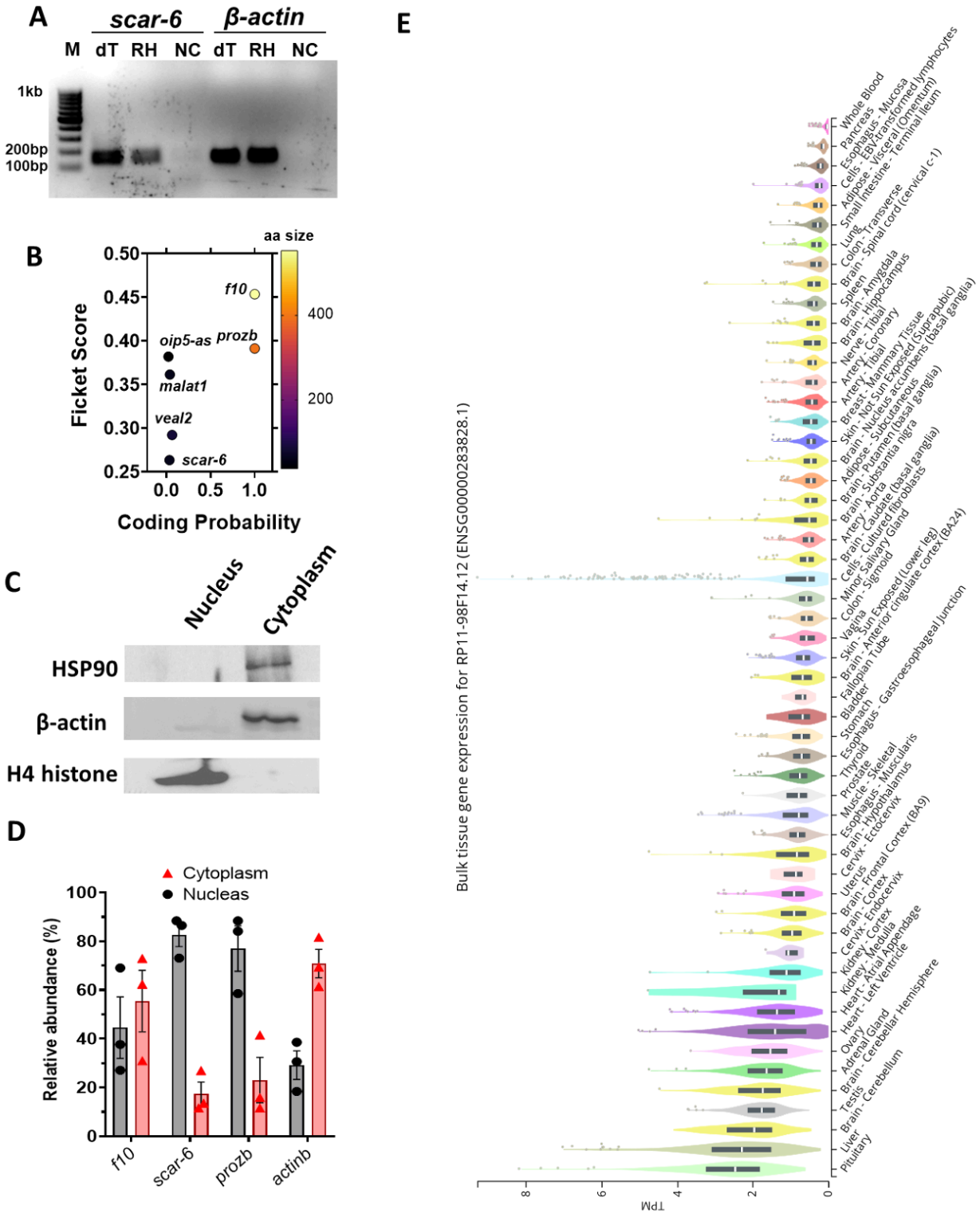

Figure EV2

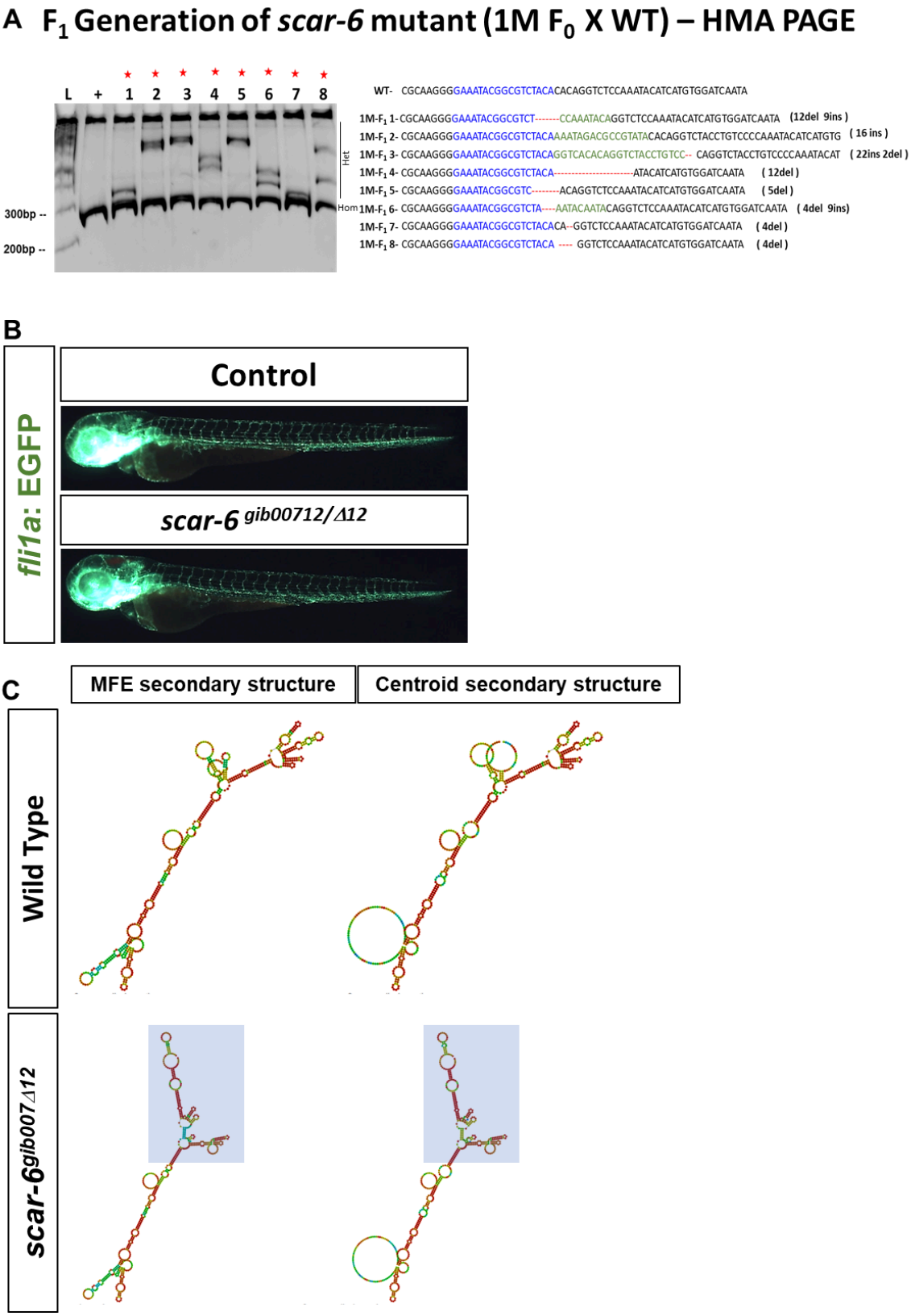

Figure EV3

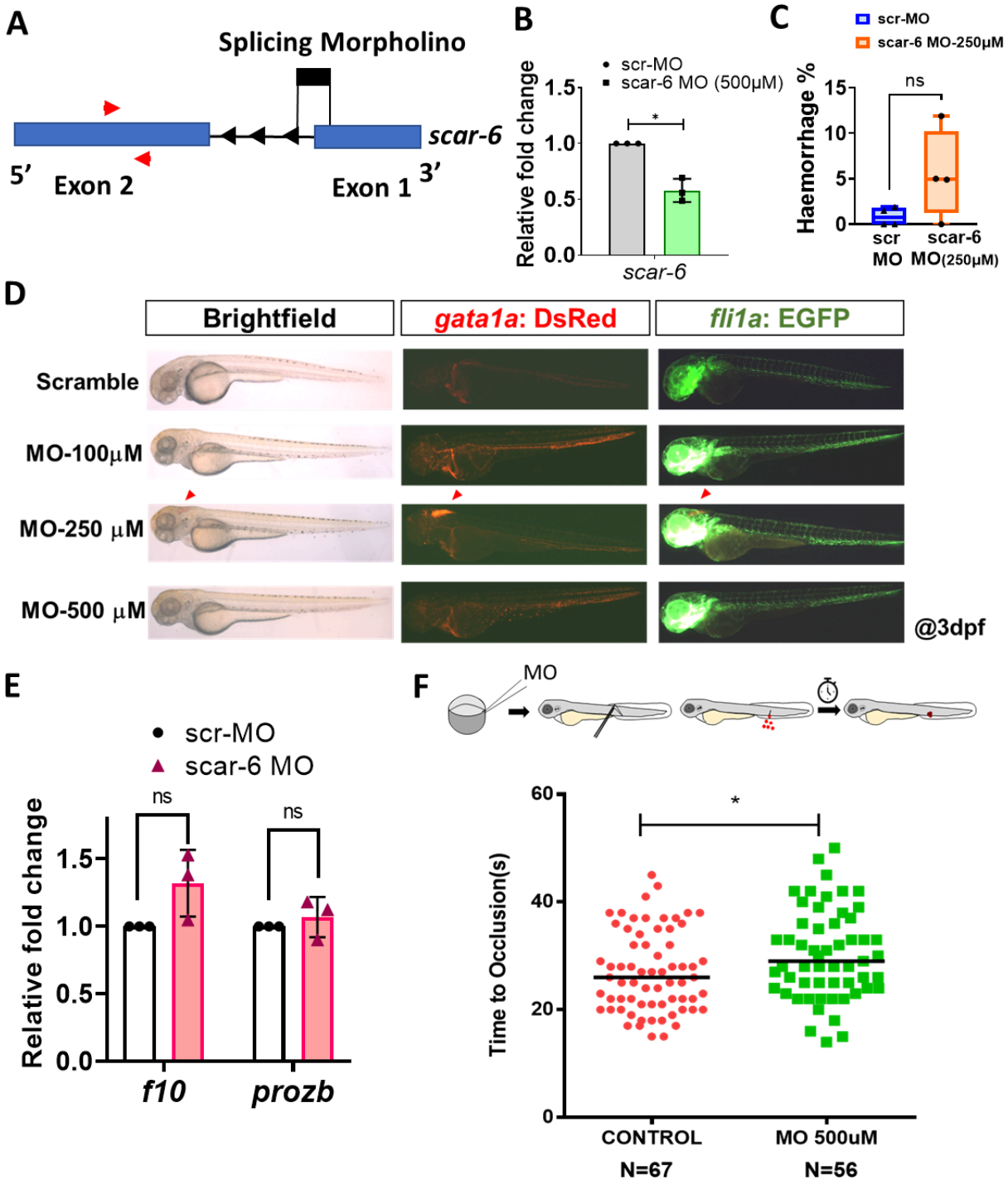

Figure EV4

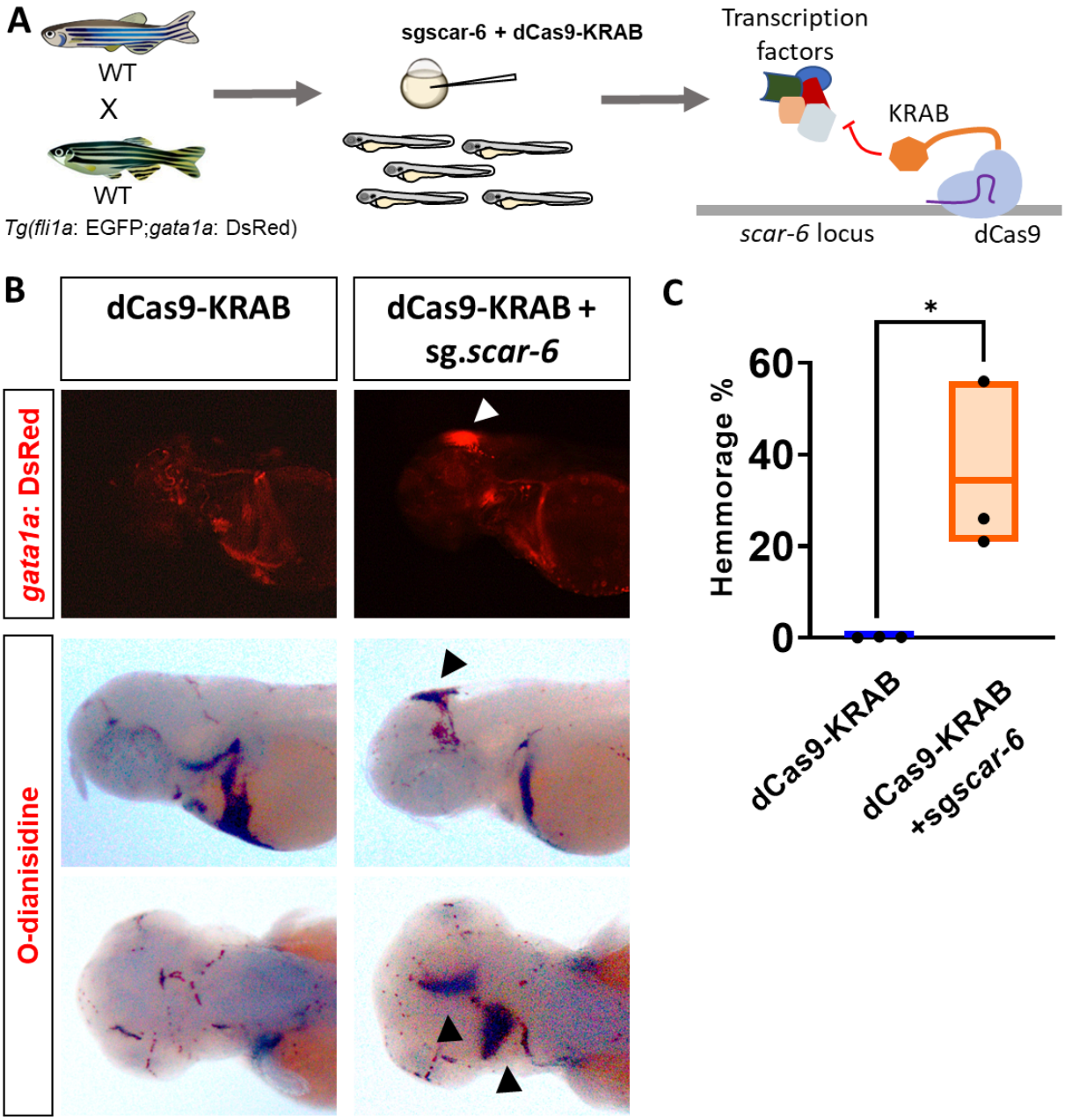

Figure EV5